RESTRICTED

RM No. E8J28d

NACA RM No. E8J28d

NACA

RESEARCH MEMORANDUM

ALTITUDE-WIND-TUNNEL INVESTIGATION OF WESTINGHOUSE 19B-2 19B-8, AND 19XB-1 JET-PROPULSION ENGINES V - COMBUSTION-CHAMBER PERFORMANCE

By Bemrose Boyd

Lewis Flight Propulsion Laboratory
Cleveland, Ohio

NATIONAL ADVISORY COMMITTEE FOR AERONAUTICS

WASHINGTON
November 26, 1948

RESTRICTED

NATIONAL ADVISORY COMMITTEE FOR AERONAUTICS

RESEARCH MEMORANDUM

ALTITUDE-WIND-TUNNEL INVESTIGATION OF WESTINGHOUSE 19B-2 19B-8, AND 19XB-1 JET-PROPULSION ENGINES V - COMBUSTION-CHAMBER PERFORMANCE

By Bemrose Boyd

SUMMARY

Pressure losses through the combustion chamber and the combustion efficiency of the 19B-2 and 19B-8 jet-propulsion engines and the combustion efficiency of the 19XB-1 jet-propulsion engine are presented. The 19B engine is one of the earliest experimental Westinghouse axial-flow engines. The 19XB-1 engine is an experimental prototype of the Westinghouse 19XB series, having a rated thrust of 1400 pounds. Improvements in performance and operational characteristics have resulted in the 19XB-2B engine with a rated thrust of 1600 pounds. Data were obtained from an investigation of the complete engine in the NACA Cleveland altitude wind tunnel over a range of simulated altitudes from 5000 to 30,000 feet and tunnel Mach numbers from less than 0.100 to 0.455.

The combustion-chamber pressure loss due to friction was higher for the 19B-2 combustion chamber than for the 19B-8. The 19B-2 combustion chamber had a screen of 40-percent open area interposed between the compressor outlet and the combustion-chamber inlet. The screen for the 19B-8 combustion chamber had a 60-percent open area, which except for a small difference in tail-pipe-nozzle outlet area represents the only point of difference between the standard 19B-2 and 19B-8 combustion chambers. The pressure loss due to heat addition to the flowing gases in the combustion chamber was approximately the same for the 19B-2 and 19B-8 configurations. Altitude and tunnel Mach number had no significant effect on the over-all total-pressure loss through the combustion chamber. A decrease in tail-pipe-nozzle outlet area (tail cone out) resulted in a decrease in combustion-chamber total-pressure loss at high engine speeds.

Combustion efficiency was slightly increased at low and medium engine speeds by increasing tunnel Mach number and was decreased at

high engine speeds by extension of the tail cone; the point of maximum efficiency was shifted to higher engine speeds by increasing altitude.

The combustion efficiency of the standard 19B-2 combustion chamber was higher than that of the 19B-8 chamber. The difference in combustion efficiencies increased with engine speed and at an altitude of 20,000 feet and a corrected engine speed of 18,000 rpm this difference was 6 percent. When the fuel-nozzle flow rating and spray angle were changed from 10.5 to 8.3 gallons per hour and from 80° to 45°, respectively, the point of maximum combustion efficiency was shifted to lower engine speeds with no change in minimum value. All other modifications (decrease in fuel-nozzle flow rating only, nozzle extensions, angle clips, and flame holder) gave efficiencies ranging from 8 to 21 percent lower than the original configurations.

The use of a high-flow compressor in the 19XB-1 configurations raised the combustion efficiency at low engine speeds and reduced the efficiency at high engine speeds with the engine operating at 20,000 feet under static conditions.

INTRODUCTION

As part of a study of performance of the 19B jet-propulsion engine components, an analysis is presented of combustion-chamber performance based on data obtained with the complete engine in the Cleveland altitude wind tunnel during October and November 1944. Results from investigations of the operational characteristics and of the performance and windmilling drag characteristics of the engine are presented in references 1 and 2, respectively. Analyses of turbine and compressor performance are given in references 3 and 4, respectively.

The variations with simulated flight conditions of the pressure losses through the combustion chamber of the 19B-8 engine and the combustion-chamber efficiency of the 19B-2, 19B-8, and 19XB-1 engine are presented herein. The pressure losses due to fluid friction and to the addition of heat to the gas flow by combustion are separately evaluated for the 19B-2 and 19B-8 engines by means of the pressure-loss chart developed in reference 5.

The engine operating range for which data are discussed extends from simulated altitudes of 5000 to 30,000 feet and tunnel Mach numbers from less than 0.100 to 0.455. These data are necessarily restricted to the operable engine speeds at each simulated altitude and tunnel speed. The fuel used was 62-octane unleaded gasoline.

Data are presented for several combustion-chamber configurations that include modifications made during the investigation. For all of the configurations except the original 19B-8, the data were taken under static conditions and at simulated altitudes of 5000 or 20,000 feet or both.

ENGINE INSTALLATION AND INSTRUMENTATION

A detailed description of the 19B and 19XB-1 engines and of the method of installation is given in reference 1. The engine was installed in a nacelle under a stub wing (fig. 1) of 7-foot span, which was supported by cantilever suspension from one side of the tunnel test section. Combustion air was admitted at the front of the nacelle and cooling air for the accessories was admitted through a small inlet duct beneath the leading edge of the wing. The tail-pipe-nozzle outlet area in the 19B-2 and 19B-8 engines was varied by means of a movable tail cone. The area variation was approximately linear with tail-cone position. In the 19B-2 engine the area could be varied from 140 square inches with the tail cone in to 112 square inches with the tail cone 4 inches out. The corresponding areas for the 19B-8 engine are 135 and 106 square inches. The 19XB-1 tail-pipe-nozzle outlet area was fixed at 103 square inches.

The engine stations at which pressure and temperature instrumentation was installed are shown in figure 2. Instrumentation at the compressor outlet and the turbine inlet is of particular importance in this report. The compressor-outlet instrumentation consisted of four static wall orifices and four rakes extending radially into the annulus, one wall orifice and one rake being located in each quadrant. The rakes in the upper right and lower left quadrants each contained three total-pressure tubes. The other two rakes each contained two thermocouples and one static-pressure tube. The turbine-inlet instrumentation consisted of a single rake located in the lower right quadrant for averaging the total pressure. Turbine-inlet total temperatures were calculated from the temperatures in the tail pipe and the temperature differences across the compressor. The compressor-inlet and tail-pipe instrumentation was similar to that at the compressor outlet, except that the rakes in all quadrants were alike and each rake contained three total-pressure tubes and two thermocouples.

DESCRIPTION OF COMBUSTION CHAMBER

The combustion chamber of the 19B and 19XB-1 engines (fig. 3) is an annulus of 19-inch outside diameter in which is mounted an

annular combustion basket (fig. 4) containing holes that distribute the combustion air to the primary and secondary burning zones. The cross-sectional area of the basket tapered from approximately 0.40 square foot at the upstream end to 1.42 square feet at a point $13\frac{3}{4}$ inches further downstream. Fuel is supplied to the combustion chamber through 24 fuel nozzles facing downstream and mounted on a circular manifold located at the upstream end of the basket. The 19B-2 and 19B-8 combustion chambers included a screen located in the compressor outlet downstream of the combustion-chamber-inlet instrumentation. In the first modification of the 19B-2 configuration (hereinafter designated 19B-2-I), the alternate fuel nozzles were extended $1\frac{1}{2}$ inches downstream and a 45° spray angle was used on the unextended nozzles. For the 19B-2-II configuration, 1/4- by 3/16-inch angle clips (fig. 5(a)) were welded to the sides of the combustion chamber $1\frac{5}{16}$ inches downstream of the fuel manifold to induce turbulence in the primary combustion zone. For the third modification of the 19B-2 engine (19B-2-III), an Inconel half-tube ring (fig. 5(b)) was mounted $2\frac{1}{2}$ inches downstream of the fuel manifold to serve as a flame holder and to provide a pilot flame to maintain combustion under altitude conditions of operation.

Differences between the various combustion-chamber configurations, including the percentage of open area of the combustion-chamber-inlet screen, and the fuel-nozzle characteristics, are summarized in the following table:

Combustion-chamber configuration	Screen open area (percent)	Fuel nozzle		Remarks
		Spray angle (deg)	Flow rating at 100 lb pressure (gal/hr)	
19B-2 original	40	80	10.5	Compressor pressure ratio, 3.5
19B-2-I	40	45, 80	10.5	Do.
19B-2-II	40	45	10.5	Do.
19B-2-III	40	45	10.5	Do.
19B-8 original	60	80	10.5	Do.
19B-8-I	60	80	8.5	Do.
19XB-1 original	---	80	10.5	Compressor pressure ratio, 4.0
19XB-1-I	---	45	8.3	Do.

SYMBOLS

The following symbols and necessary values are used in the computations:

A	area of cross section of equivalent combustion chamber, square feet
A_1	area of cross section of cowling inlet, square feet
$c_{p,1}$	specific heat at constant pressure at cowling inlet, Btu per pound $^{\circ}R$
$c_{p,b}$	average specific heat at constant pressure for combustion chamber, Btu per pound $^{\circ}R$
$c_{p,c}$	average specific heat at constant pressure for compressor, Btu per pound $^{\circ}R$
$c_{p,t}$	average specific heat at constant pressure for turbine, Btu per pound $^{\circ}R$
h	lower heating value of fuel, 18,600 Btu per pound
J	mechanical equivalent of heat, 778 foot-pounds per Btu
K	combustion-chamber friction-pressure-loss factor
M	Mach number
N	engine speed, rpm
P	total pressure, pounds per square foot absolute
ΔP_F	loss in total pressure due to friction, pounds per square foot
ΔP_M	loss in total pressure due to addition of heat to flowing gas by combustion (momentum-pressure loss), pounds per square foot
ΔP_T	over-all loss in total pressure due to friction and addition of heat by combustion, pounds per square foot
p	static pressure, pounds per square foot absolute
R	gas constant for air, 53.3 foot-pounds per pound $^{\circ}R$

T total temperature, °R

T_i indicated temperature, °R

ΔT_c temperature rise across compressor, °R

ΔT_t temperature drop across turbine, °R

t static temperature, °R

V linear velocity, feet per second

W_a air flow, pounds per second

W_f fuel flow, pounds per second

α thermocouple impact-recovery factor, 0.85

γ ratio of specific heat at constant pressure to specific heat at constant volume

η_b combustion-chamber efficiency, percent

θ ratio of cowling-inlet total temperature to NACA standard static temperature at sea level

ρ air density, pounds per cubic foot

Subscripts:

0 free stream

1 cowling inlet

2 compressor inlet

3 compressor outlet (combustion-chamber inlet)

4 turbine inlet (combustion-chamber outlet)

5 turbine outlet (tail pipe)

6 tail-pipe-nozzle outlet

B entrance to combustion zone

b combustion chamber

c compressor

t turbine

METHODS OF ANALYSIS

Total-pressure loss across combustion chamber. - The over-all total-pressure loss across the combustion chamber was obtained from the difference in total pressure measured at the turbine inlet, station 4, and the compressor outlet, station 3. The method and the chart given in reference 5 were used to determine that part of the total-pressure loss due to friction ΔP_F and that part due to the addition of heat to the gases in the combustion chamber ΔP_M. All the friction pressure loss is assumed to occur before the gas becomes involved in combustion. The over-all pressure loss ΔP_T is the sum of the friction-pressure loss ΔP_F and the momentum-pressure loss ΔP_M

$$\Delta P_T = \Delta P_F + \Delta P_M \tag{1}$$

By means of the chart of reference 5, the friction- and momentum-pressure losses can be specified by two quantities that are characteristic of the combustion chamber: the friction-pressure-loss factor K and the equivalent area of cross section A. The factor K is related to the friction-pressure loss by means of the equation

$$\Delta P_F = KR \frac{W_a^2 T_3}{P_3} \tag{2}$$

The equivalent area A is the cross section of a corresponding combustion chamber of constant cross-sectional area with the same momentum-pressure-loss characteristics as the actual combustion chamber.

The values of K and A for the 19B-2 and 19B-8 combustion chambers were determined over a range of values of measured pressure losses corresponding to the range of engine operating conditions investigated.

Combustion-chamber efficiency. - The combustion-chamber efficiency η_b is defined as the ratio of the actual enthalpy rise of the gases across the combustion chamber to the theoretical enthalpy rise that would be realized with complete combustion

$$\eta_b = \frac{c_{p,b}(T_4-T_3)}{h(W_f/W_a)} \tag{3}$$

No correction was made for the heat losses from the combustion chamber by radiation and conduction.

METHODS OF CALCULATION

Air flow. - The air flow through the combustion chamber was determined from temperature and pressure measurements obtained at the cowling inlet by means of the following equations:

$$W_a = \rho_1 A_1 V_1 \tag{4}$$

$$\rho_1 = \frac{p_1}{Rt_1} \tag{5}$$

$$A_1 = 1.069$$

$$V_1 = \sqrt{64.4\ Jc_{p,1}t_1\left[\left(\frac{P_1}{p_1}\right)^{\frac{\gamma-1}{\gamma}} - 1\right]} \tag{6}$$

Temperatures. - Total temperatures were calculated from indicated temperature readings by

$$T = \frac{T_i\left(\frac{P}{p}\right)^{\frac{\gamma-1}{\gamma}}}{1 + \alpha\left[\left(\frac{P}{p}\right)^{\frac{\gamma-1}{\gamma}} - 1\right]} \tag{7}$$

The recovery factor α was taken equal to 0.85.

The turbine-inlet (combustion-chamber outlet) total temperature T_4 was computed from the tail-pipe indicated temperature $T_{i,5}$ by equation (7) and the following equation:

$$T_4 = T_5 + \Delta T_t \tag{8}$$

On the assumption that the enthalpy rise across the compressor $c_{p,c}\Delta T_c$ is equal to the enthalpy drop across the turbine $\left(1 + \frac{W_f}{W_a}\right) c_{p,t}\Delta T_t$, the value of ΔT_t is obtained

$$\Delta T_t = \frac{c_{p,c}\Delta T_c}{c_{p,t}\left(1 + \frac{W_f}{W_a}\right)} \tag{9}$$

RANGE OF DATA

The combustion-chamber data discussed are restricted to the operable range of engine speeds corresponding to the simulated altitudes and flight speeds. The characteristic quantities K and A were evaluated for the 19B-2 and 19B-8 engines. Experimental data with all modified combustion chambers were taken only for the static case (tunnel Mach number less than 0.100); therefore all comparisons among combustion chambers are limited to this case. Data for the configurations involved in these comparisons were obtained at simulated altitudes of 5000 or 20,000 feet or both.

RESULTS AND DISCUSSION

Combustion-Chamber Pressure Losses

The cycle efficiency of a turbojet engine is adversely affected by any loss in total pressure through the combustion chamber (references 5 and 6). Thus the variation of combustion-chamber total-pressure loss with operating conditions is important to the over-all performance of the engine.

Measured pressure losses. - The pressure-loss data presented in figures 6 to 8 are for the 19B-8 engine.

The variation of measured over-all total-pressure-loss ratio $\Delta P_T/P_3$ with corrected engine speed $N/\sqrt{\theta}$ for a range of simulated

altitudes from 5000 to 30,000 feet and average tunnel Mach numbers of less than 0.100, 0.147, and 0.431 is shown in figure 6. No effect of altitude on $\Delta P_T/P_3$ was obtained except possibly a very slight effect at the highest Mach number. The peak value of $\Delta P_T/P_3$ was 0.089 at an average tunnel Mach number of 0.431 and a corrected engine speed of 17,000 rpm (fig. 6(c)).

The variations of $\Delta P_T/P_3$ with corrected engine speed for a range of tunnel Mach numbers from less than 0.100 to 0.455, at simulated altitudes of 5000 feet with tail cone in and 15,000 feet with tail cone 4 inches out are shown in figures 7(a) and 7(b), respectively. Tunnel Mach number had no measurable consistent effect on $\Delta P_T/P_3$ at either altitude and tail-cone setting.

The variation of $\Delta P_T/P_3$ with corrected engine speed for setting of the tail cone in and 4 inches out at simulated altitudes and average tunnel Mach numbers of 10,000 feet and 0.269, 10,000 feet and 0.420, and 15,000 feet and 0.147 are shown in figures 8(a), 8(b), and 8(c), respectively. Reduction of the tail-pipe area (tail cone out) had no effect on $\Delta P_T/P_3$ below a corrected engine speed of 15,000 rpm, but did give reduced values of $\Delta P_T/P_3$ above this engine speed. At a corrected engine speed of 17,000 rpm, the value of $\Delta P_T/P_3$ with the tail cone 4 inches out was approximately 20 percent below that obtained with the tail cone in. The reduced values of $\Delta P_T/P_3$ result from the lowered air mass flow through the engine accompanying the reduction in exhaust-nozzle area. This effect will be subsequently explained in greater detail.

Calculated friction- and momentum-pressure losses. - The friction-pressure loss and the pressure loss due to heat addition by fuel combustion to the air flowing in the combustion chamber (momentum-pressure loss) were obtained from the pressure-loss chart (fig. 9) according to the method described in the appendix. The values of the friction-pressure-loss factor K and the equivalent cross-sectional area A required to obtain the momentum-pressure loss were obtained from measured pressure-loss data according to the methods described in reference 5. The value of K was found to be constant for a given combustion chamber over the entire range of values of the combustion-chamber-entrance parameter $W_a\sqrt{T_3}/P_3$. The value of A was found to be constant at 0.68 square foot up to a value of $W_a\sqrt{T_3}/P_3$ of 0.115. In the range of values of $W_a\sqrt{T_3}/P_3$ from 0.115 to 0.129, the value of A decreases with increasing $W_a\sqrt{T_3}/P_3$ to a minimum value of 0.518, as shown in figure 10. The

variation in the value of A with $W_a\sqrt{T_3}/P_3$ is attributed to changes in the flame configurations occurring in this range of values of $W_a\sqrt{T_3}/P_3$. Above a value of 0.129 for $W_a\sqrt{T_3}/P_3$, A reassumes its constant value of 0.68. In the range of values of $W_a\sqrt{T_3}/P_3$ for which A varies, the constant value may also occur. For this range either of two values of the momentum-pressure loss and of the over-all pressure loss corresponding to the two possible values of A may be computed.

In the curves showing the variation of $\Delta P_T/P_3$ with engine operating conditions, $\Delta P_T/P_3$ is plotted against corrected engine speed $N/\sqrt{\theta}$. The variation of A was, however, determined as a function of $W_a\sqrt{T_3}/P_3$. Therefore, in order to correlate the air flow and the pressure losses more easily, the variation of $W_a\sqrt{T_3}/P_3$ with $N/\sqrt{\theta}$ is given in figure 11 for the same engine and conditions of operation for which data are given in figure 12.

A comparison between measured over-all total-pressure-loss ratios $\Delta P_T/P_3$ and calculated values obtained by applying the pressure-loss chart to experimental data from the 19B-8 engine is given in figure 12. The curves shown were selected to illustrate a variety of effects that result from having two possible values of A, one constant and the other variable, for a limited range of values of $W_a\sqrt{T_3}/P_3$. In each part of the figure, calculated pressure losses are given for the constant value of A and for values of A varying according to figure 10 in the applicable range of $W_a\sqrt{T_3}/P_3$. The experimental values of $\Delta P_T/P_3$ approximate either those given by a constant value of A or those obtained with a variable value of A. In figure 12 the values of friction-pressure-loss ratio $\Delta P_F/P_3$ obtained from the pressure-loss chart of figure 9 are also plotted. The difference between $\Delta P_T/P_3$ and $\Delta P_F/P_3$ is equal to the momentum-pressure-loss ratio $\Delta P_M/P_3$. In general, the momentum-pressure loss varies from about 1.2 to 2.3 times the value of the friction-pressure loss.

The curves of figure 12(a) were obtained with the 19B-8 combustion chamber at a tunnel Mach number of 0.142 and a simulated altitude of 5000 feet with the tail cone in. At a corrected engine speed of 10,250 rpm, branching of the calculated $\Delta P_T/P_3$ curve occurs. The upper branch of the curve corresponds to variable values of A and the lower branch to constant values. The measured pressure losses persist along the lower branch of the calculated

curve, corresponding to a constant value of A, up to a corrected engine speed of 12,700 rpm. For higher engine speeds, the measured data are in agreement with the branch of the curve calculated for a varying value of A.

In figure 12(c) the curves for constant A and for variable A join at the high-engine-speed end. These data were obtained with the 19B-8 combustion chamber operating at a simulated altitude of 25,000 feet and a tunnel Mach number of 0.153 with the engine tail cone in. Except at the data point for 18,750 rpm, the measured values of $\Delta P_T/P_3$ follow the branch of the calculated curve for variable values of A. The data for this set of operating conditions do not extend to corrected engine speeds below 17,000 rpm.

Data for the same engine configuration and a simulated altitude of 5000 feet for a tunnel Mach number of 0.298 are shown in figure 12(d). The upper branch of the calculated curve is discontinuous at values of $N/\sqrt{\theta}$ equal to 11,100 and 15,600. Data for this case in figure 11 show that for corrected engine speeds between 11,100 and 15,600 rpm the values of $W_a\sqrt{T_3}/P_3$ are greater than 0.129 and, consequently, the constant value of A (0.68 sq ft) should apply; whereas for engine speeds either above or below this range, the values of $W_a\sqrt{T_3}/P_3$ lie between 0.155 and 0.129 and variable values of A may be applicable. In the low-engine-speed range, the experimental data correspond to the calculations based on a constant value of A, although values corresponding to variable values of A are also possible. In the intermediate range of engine speeds, the measured pressure losses (fig. 12(d)) also agree with the calculations based on a constant value of A; whereas for the high-speed range, the experimental data correspond to calculations based on a variable A.

A type of branching of the calculated values of $\Delta P_T/P_3$ in which the curve for the variable values of A is joined at both ends to the curve for constant value of A is shown in figure 12(e). That such a form of the calculated curve is probable is indicated by the data for this case in figure 11, where only the values of $W_a\sqrt{T_3}/P_3$ for the intermediate corrected-engine-speed range lie within the range in which variable values of A may occur. These data were taken with the 19B-8 combustion chamber operating at a simulated altitude of 15,000 feet and a tunnel Mach number of 0.147 with the tail cone extended 4 inches.

The effect of tail-cone position on measured pressure loss at high engine speeds observed in figure 8 can be explained by referring to figures 11, 12(b), and 12(e). The reduction of exit area

results in a smaller $W_a\sqrt{T_3}/P_3$ for a given engine speed (fig. 11), which produces a slightly lower friction-pressure drop and a shift to a higher (constant) value of A and therefore a lower momentum-pressure drop. This effect is absent in the low range of engine speeds, because in that region $W_a\sqrt{T_3}/P_3$ is not influenced to a significant degree by variations in tail-cone position.

In general, when values of pressure loss for both constant and variable A are theoretically possible, the experimental values correspond to the theoretical values calculated for constant A at low engine speeds and to those for variable A at high engine speeds. This effect is seen in figures 12(a), 12(b), 12(d), and 12(e).

The following values of K, A, and KA^2 were obtained for the unmodified 19B-2 and 19B-8 combustion chambers from measured combustion-chamber pressure losses by means of the pressure-loss chart of figure 9:

Combustion chamber	Screen open area (percent)	K	A	KA^2
19B-2	40	0.038	0.68	0.018
19B-8	55	.032	.68	.015

Inasmuch as K is larger for the 19B-2, the friction-pressure loss is greater for that combustion chamber. The value of A is for the range in which A remains constant. The variation of A with $W_a\sqrt{T_3}/P_3$ for the 19B-8 combustion chamber is shown in figure 10. The actual combustion-chamber basket tapered from an area of approximately 0.40 square foot at the upstream end to 1.42 square feet at the downstream end.

Combustion Efficiency

The combustion efficiency for most operating conditions with unmodified combustion chambers had a maximum value of approximately 96 percent and did not fall below 75 percent within the operating range. The minimum value including modifications was 62 percent and the modified configurations had lower peaks. Thus the total variation of efficiency over the entire range of operating conditions covered in any test was small.

Effect of engine operating conditions. - The effect of engine operating conditions on combustion efficiency is presented for the 19B-8 turbojet engine. The variation of combustion efficiency with simulated altitudes at average tunnel Mach numbers of less than 0.100 and 0.431 is presented in figures 13(a) and 13(b), respectively.

The maximum combustion efficiency attained at a given altitude decreased with increasing altitude except at 30,000 feet. The corrected engine speed at which maximum combustion efficiency was obtained increased with increasing altitude. For a tunnel Mach number of less than 0.100 (fig. 13(a)), a maximum combustion efficiency of 92 percent at 5000 feet was obtained at a corrected engine speed of 14,000 rpm; whereas at 20,000 feet a maximum combustion efficiency of approximately 88 percent was obtained at an engine speed of about 16,500 rpm. In general, the rate of change of combustion efficiency with engine speed for engine speeds below that corresponding to peak efficiency increased with increasing altitude.

The effect of tunnel Mach number on combustion efficiency is shown in figure 14 for operation at a simulated altitude of 5000 feet with the tail cone in and at 15,000 feet with the tail cone 4 inches out. At Mach numbers of 0.147 and above, the combustion efficiency increased with tunnel Mach number for values of corrected engine speed below about 17,000 rpm. Below a Mach number of 0.147 the relation is confused by the scatter of experimental data. At a corrected engine speed of 14,000 rpm and an altitude of 5000 feet (fig. 14(a)), the combustion efficiency increased from a value of approximately 91 percent at a tunnel Mach number of 0.142 to 95.5 percent at a tunnel Mach number of 0.298. For the same engine speed and an altitude of 15,000 feet (fig. 14(b)), the combustion efficiency increased from a value of 86 percent at a tunnel Mach number of 0.147 to 94 percent at a tunnel Mach number of 0.455. The value of 75 percent at 15,000 feet and 8800 rpm was the lowest efficiency recorded with any unmodified configuration (fig. 14(b)).

The effect of tail-cone position on combustion efficiency is shown in figure 15. The data were obtained with the unmodified 19B-8 combustion chamber at a simulated altitude of 10,000 feet and tunnel Mach numbers of 0.269 and 0.420. Except at the low corrected engine speeds, a decrease in the tail-pipe-nozzle outlet area (tail cone out) resulted in a decrease in combustion efficiency. The magnitude of the decrease became greater as the engine speed was increased. At a corrected engine speed of 17,000 rpm, the combustion efficiency was 8 or 9 percent higher with the tail cone in than with the tail cone 4 inches out.

Effect of engine configuration. - The improvement in combustion efficiency obtained with a screen having a 40-percent open area placed between the combustion-chamber inlet and the combustion zone (19B-2 combustion chamber) over a screen with a 60-percent open area (19B-8 combustion chamber) is shown in figure 16 for simulated altitudes of 5000 and 20,000 feet. The differences shown are assumed to be due largely to the different screens although a 3.5-percent difference in tail-pipe-nozzle outlet area is also involved. Operation of the combustion chamber with the screen having a 40-percent open area gave a combustion efficiency of 96 percent and the screen with a 60-percent open area gave a 91-percent combustion efficiency at a corrected engine speed of 15,000 rpm and an altitude of 5000 feet (fig. 16(a)). At an altitude of 20,000 feet and a corrected engine speed of 18,000 rpm, the 19B-8 efficiency was 87 percent and decreased as the engine speed increased; whereas the 19B-2 efficiency was 93 percent and increased with engine speed. In the low-engine-speed range, both combustion chambers gave about the same efficiency. The value of 96 percent for the 19B-2 configuration at 15,000 rpm was the highest recorded efficiency.

The effect of fuel-nozzle extensions on the combustion efficiency of the 19B-2 combustion chamber operating at a simulated altitude of 5000 feet and a tunnel Mach number less than 0.100 is shown in figure 17. Extension of the fuel nozzles gave combustion efficiencies of about 11 to 17 percent less than those obtained with the standard fuel nozzles.

Angle clips reduced the combustion efficiency of the 19B-2 combustion chamber by an average of about 9 percent in the range of corrected engine speeds from 11,000 to 15,000 rpm (fig. 18) and the reduction increased to about 18 percent at a corrected engine speed of 8000 rpm. The data were obtained at a simulated altitude of 5000 feet and a tunnel Mach number of less than 0.100.

The use of a half-tube flame holder in the 19B-2 combustion chamber gave a reduction in combustion efficiency ranging from 21 percent at a corrected engine speed of 7750 rpm to 12 percent at an engine speed of 15,000 rpm (fig. 19). These data were obtained at a simulated altitude of 5000 feet and a tunnel Mach number of less than 0.100. The value of 62 percent for the modified configuration at 7600 rpm was the lowest efficiency recorded.

A reduction in the fuel-nozzle flow rating (arbitrary rating at 100 lb pressure) from 10.5 to 8.5 gallons per hour reduced the combustion efficiency of the 19B-8 combustion chamber by 8 to 11 percent in the limited range of corrected engine speeds for which the

data in figure 20 were obtained. These data were obtained at a simulated altitude of 5000 feet and a tunnel Mach number of less than 0.100. The improvement in the degree of fuel-droplet disintegration obtained with the 8.5-gallon-per-hour fuel nozzle did not give the expected rise in combustion efficiency. However, a change in both flow capacity and spray angle from 10.5 to 8.3 gallons per hour and 80° to 45° (fig. 21) raised the combustion efficiency of the 19XB-1 combustion chamber in the low range of corrected engine speeds. At an engine speed of 10,650 rpm, the combustion efficiency was 84 percent with the standard nozzle (10.5 gal/hr) and 90 percent with the low-flow nozzle (8.3 gal/hr) for operation at an altitude of 20,000 feet and a tunnel Mach number of less than 0.100. Above an engine speed of 14,000 rpm, the low-flow nozzles gave lower combustion efficiencies than the standard nozzles.

The 19XB-1 combustion chamber with no screen at the compressor outlet and a compressor pressure ratio of 4.0 gave higher combustion efficiencies than the same combustion chamber in the 19B-2 engine with a screen and a compressor pressure ratio of 3.5 at corrected engine speeds less than 16,100 rpm, a simulated altitude of 20,000 feet, and a Mach number of less than 0.100 (fig. 22). The tail-cone position of the 19B-2 was adjusted to give approximately the same nozzle-outlet area as the 19XB-1. The combustion chamber failed to develop the turbine-inlet temperature necessary in the 19B-2 engine to permit operation at speeds below 15,500 rpm; whereas operation with the 19XB-1 engine was possible at speeds as low as 10,500 rpm. Above an engine speed of 16,000 rpm, the 19B-2 engine gave higher combustion efficiencies than the 19XB-1. Under these conditions (simulated altitude, 20,000 feet; Mach number, less than 0.100), the combustion-chamber efficiency of the 19XB-1 reached a peak of 91 percent at 14,750 rpm; whereas the 19B-2 efficiency at 18,000 rpm (the highest engine speed attained during this run) was 96 percent and was still rising.

SUMMARY OF RESULTS

The following results were obtained from operation of the 19B-8 combustion chamber in the complete engine at tunnel Mach numbers from less than 0.100 to 0.455 and simulated altitudes from 5000 to 30,000 feet and from operation of the 19B-2, 19XB-1, and all modifications in the complete engines under static conditions and at altitudes of 5000 or 20,000 feet or both:

1. The available data showed no significant effect of altitude or tunnel Mach number on the over-all combustion-chamber total-pressure-loss ratio $\Delta P_T/P_3$. Tail-cone extension had no effect at low engine speeds but caused lower pressure losses at high engine speeds. The decrease was approximately 20 percent at a corrected engine speed of 17,000 rpm for a tail-cone extension of 4 inches, which is equivalent to a reduction inttail-pipe-nozzle outlet area from 135 to 106 square inches.

2. For values of the combustion-chamber-entrance parameter $W_a\sqrt{T_3}/P_3$ from 0.115 to 0.129, the equivalent area of cross section A, related to the momentum-pressure losses, was double valued. In addition to the value of A, which was constant for all values of $W_a\sqrt{T_3}/P_3$, a smaller value of A may be encountered in this range of values of $W_a\sqrt{T_3}/P_3$. The smaller value of A corresponded to a higher value of the momentum-pressure loss than was obtained for the constant value of A.

From the measured pressure losses, the following values of the friction-pressure-loss coefficient K and the constant equivalent area of cross section A were obtained:

Combustion chamber	K	A	KA^2
19B-2	0.038	0.68	0.018
19B-8	.032	.68	.015

The friction-pressure loss was greater for the 19B-2 combustion chamber than for the 19B-8.

3. The engine speed at which the peak combustion efficiency occurred increased as the simulated altitude was increased. The values of these peak efficiencies varied inversely with altitude with the exception of points at 30,000 feet. The rate of change of efficiency with engine speed at speeds below that corresponding to peak efficiency increased with increasing altitude. The highest combustion efficiency for the 19B-8 engine was 95.5 percent and was attained at 14,000 rpm, a tunnel Mach number of 0.298, and a simulated altitude of 5000 feet. The 19B-2 engine attained a maximum combustion efficiency of 96 percent under static conditions at 5000 feet and 15,000 rpm with the tail cone in and at 20,000 feet and 18,000 rpm with the tail cone 4 inches out. The highest efficiency for the 19XB-1 combustion chamber was 91 percent at 20,000 feet and 14,750 rpm.

4. Increasing tunnel Mach number, in general, produced an increase in combustion efficiency in the low and medium range of engine speeds. At 14,000 rpm and 15,000 feet with the tail cone 4 inches out, the efficiency increased 8 percent from a Mach number of 0.147 to 0.455.

5. A loss of combustion efficiency resulted from extension of the tail cone (decrease in tail-pipe-nozzle outlet area). This loss was equal to 8 or 9 percent at 17,000 rpm for a 4-inch extension of the tail cone and became greater as engine speed was increased.

6. The efficiency of the 19B-8 combustion chamber with an inlet screen having an open area of 60 percent was 6 percent lower than that of the 19B-2 combustion chamber with a screen open area of 40 percent at a corrected engine speed of 18,000 rpm and an altitude of 20,000 feet. Both combustion chambers gave about the same efficiency in the low engine-speed range.

7. At low engine speeds, the combustion efficiency was higher for the 19XB-1 engine with a compressor pressure ratio of 4.0 than for the 19B-2 engine with a compressor pressure ratio of 3.5. At high engine speeds the reverse was true. The highest efficiency recorded for the 19B-2 was 5 percent above the 19XB-1 maximum efficiency.

8. When the fuel-nozzle flow rating and spray angle were changed from 10.5 to 8.3 gallons per hour and from 80° to 45°, respectively, the point of maximum combustion efficiency was shifted to lower engine speeds with no change in maximum value.

9. All other modifications (decrease in fuel-nozzle flow rating only, nozzle extensions, angle clips, and flame holder) gave efficiencies ranging from 8 to 21 percent lower than the original configurations.

Lewis Flight Propulsion Laboratory,
National Advisory Committee for Aeronautics,
Cleveland, Ohio.

APPENDIX - USE OF PRESSURE-LOSS CHART

The pressure-loss chart (fig. 9) described in detail in reference 5 was developed on the basic assumption that the actual combustion-chamber pressure losses can be matched by those of an equivalent combustion chamber of constant cross-sectional area A in which all the friction-pressure drop occurs ahead of the combustion zone. The friction- and momentum-pressure losses are thus separated and equation (1) is assumed to hold. Inasmuch as P_B, the total pressure at the boundary between the friction and combustion zones of the equivalent combustion chamber, is nearly equal to P_3

$$\frac{\Delta P_F}{P_3} + \frac{\Delta P_M}{P_B} = \frac{\Delta P_T}{P_3}$$

The values of K and A for a given combustion chamber can be determined by means of the chart if $\Delta P_T/P_3$, $\Delta P_F/P_3$, and T_4/T_3 are known from experiment for the same value of $W_a\sqrt{T_3}/P_3$. The friction-pressure loss ΔP_F is measured across the entire combustion chamber with air flowing through the combustion chamber without combustion taking place (engine windmilling). A value of $\Delta P_M/P_3$ from equation (1) and T_4/T_3 determine a value of M_B in quadrant III. This value of M_B and the known value of $\Delta P_F/P_3$ determine M_3 in quadrant II. The value of M_3 thus obtained and $\Delta P_F/P_3$ in quadrant I determine a value of KA^2; M_3 and $W_a\sqrt{T_3}/P_3$ in quadrant IV determine A.

Once the values of K and A for the combustion chamber are known, the values of $\Delta P_F/P_3$ and $\Delta P_M/P_B$ for known values of the combustion-chamber-inlet parameter $W_a\sqrt{T_3}/P_3$ and the total-temperature ratio T_4/T_3 may be obtained from the chart. With $W_a\sqrt{T_3}/P_3$ and A known in quadrant IV, M_3 is determined. The known KA^2 and M_3 in quadrant I give $\Delta P_F/P_3$. The values of $\Delta P_F/P_3$ and M_3 in quadrant II give M_B. This value of M_B and T_4/T_3 in quadrant III determine $\Delta P_M/P_B$. The sum of $\Delta P_F/P_3$ and $\Delta P_M/P_B$ is $\Delta P_T/P_3$.

REFERENCES

1. Fleming, William A.: Altitude-Wind-Tunnel Investigation of Westinghouse 19B-2, 19B-8, and 19XB-1 Jet-Propulsion Engines. I - Operational Characteristics. NACA RM No. E8J28, 1948.

2. Fleming, William A., and Dietz, Robert O., Jr.: Altitude-Wind-Tunnel Investigation of Westinghouse 19B-2, 19B-8, and 19XB-1 Jet-Propulsion Engines. III - Performance and Windmilling Drag Characteristics. NACA RM No. E8J28b, 1948.

3. Krebs, Richard P., and Suozzi, Frank L.: Altitude-Wind-Tunnel Investigation of Westinghouse 19B-2, 19B-8, and 19XB-1 Jet-Propulsion Engines. II - Analysis of Turbine Performance of 19B-8 Engine. NACA RM No. E8J28a, 1948.

4. Dietz, Robert O., and Kuenzig, John K.: Altitude-Wind-Tunnel Investigation of Westinghouse 19B-2, 19B-8, and 19XB-1 Jet-Propulsion Engines. IV - Analysis of Compressor Performance. NACA RM No. E8J28c, 1948.

5. Pinkel, I. Irving, and Shames, Harold: Analysis of Jet-Propulsion Engine Combustion-Chamber Pressure Losses. NACA TN No. 1180, 1947.

6. Pinkel, I. Irving, and Shames, Harold: Altitude-Wind-Tunnel Investigation of a 4000-Pound-Thrust Axial-Flow Turbojet Engine. VI - Combustion-Chamber Performance. NACA RM No. E8F09e, 1948.

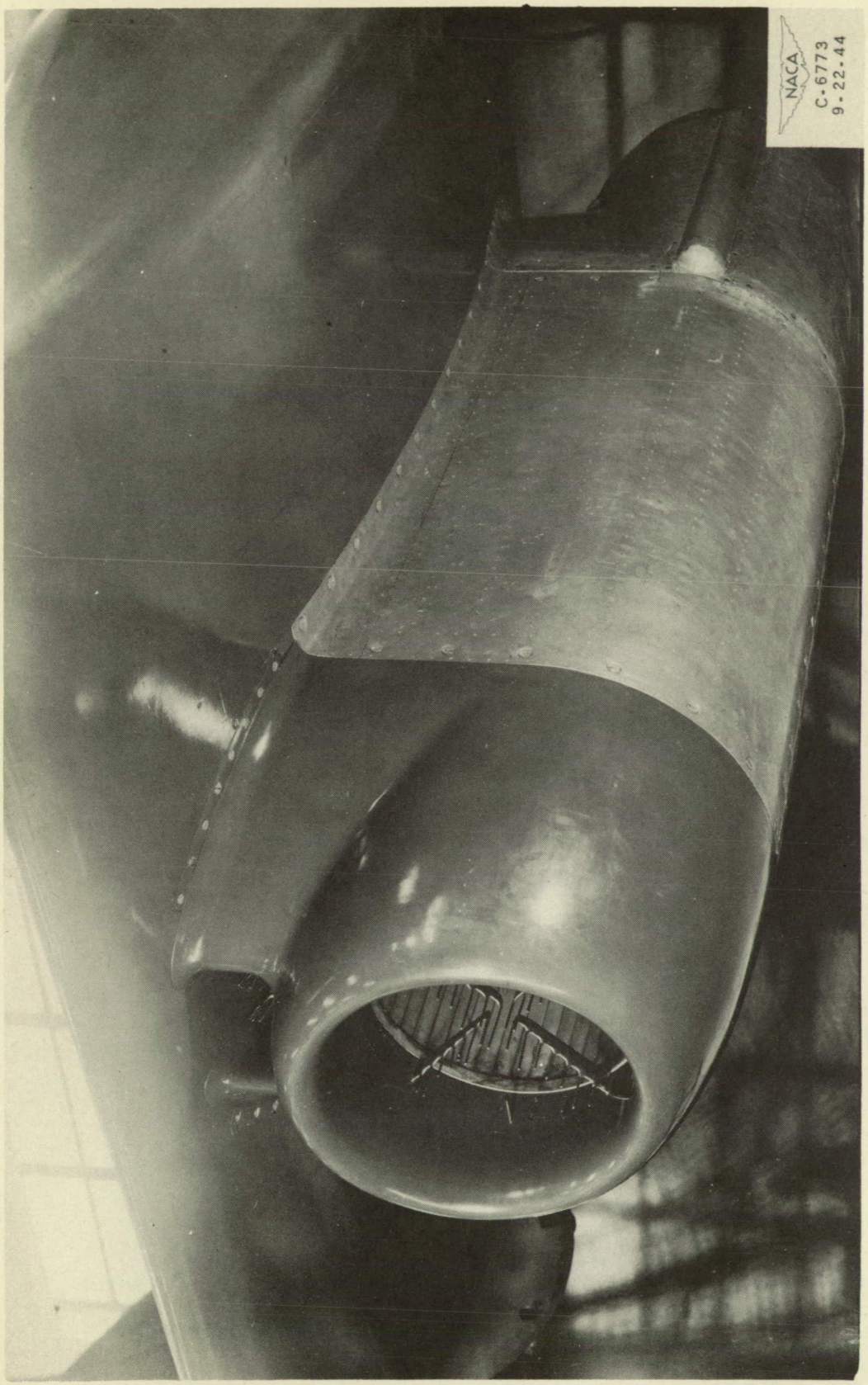

Figure 1. - Installation of 198 jet-propulsion engine in wing nacelle for investigation in altitude wind tunnel.

Page intentionally left blank

Page intentionally left blank

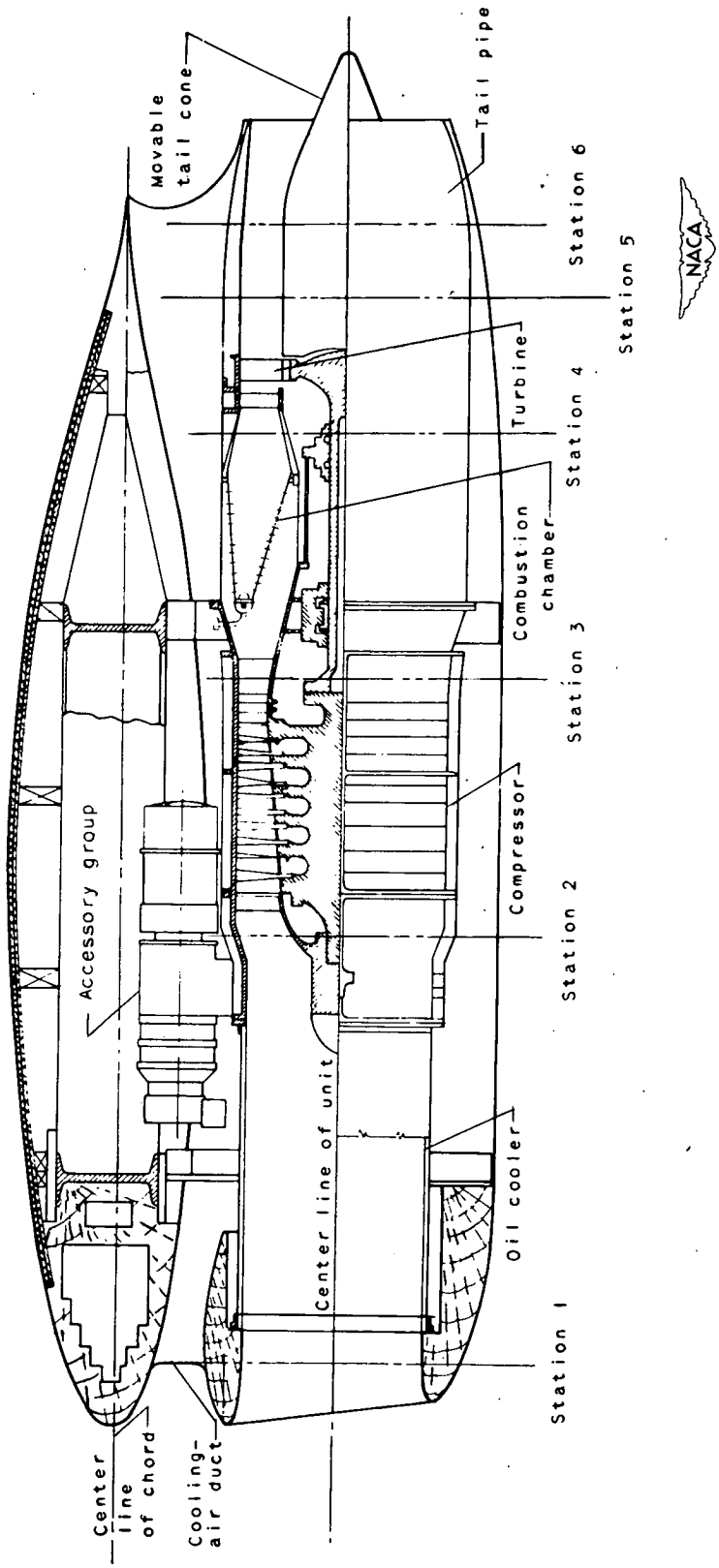

Figure 2. - Schematic view of 19B jet-propulsion engine installation showing measuring stations.

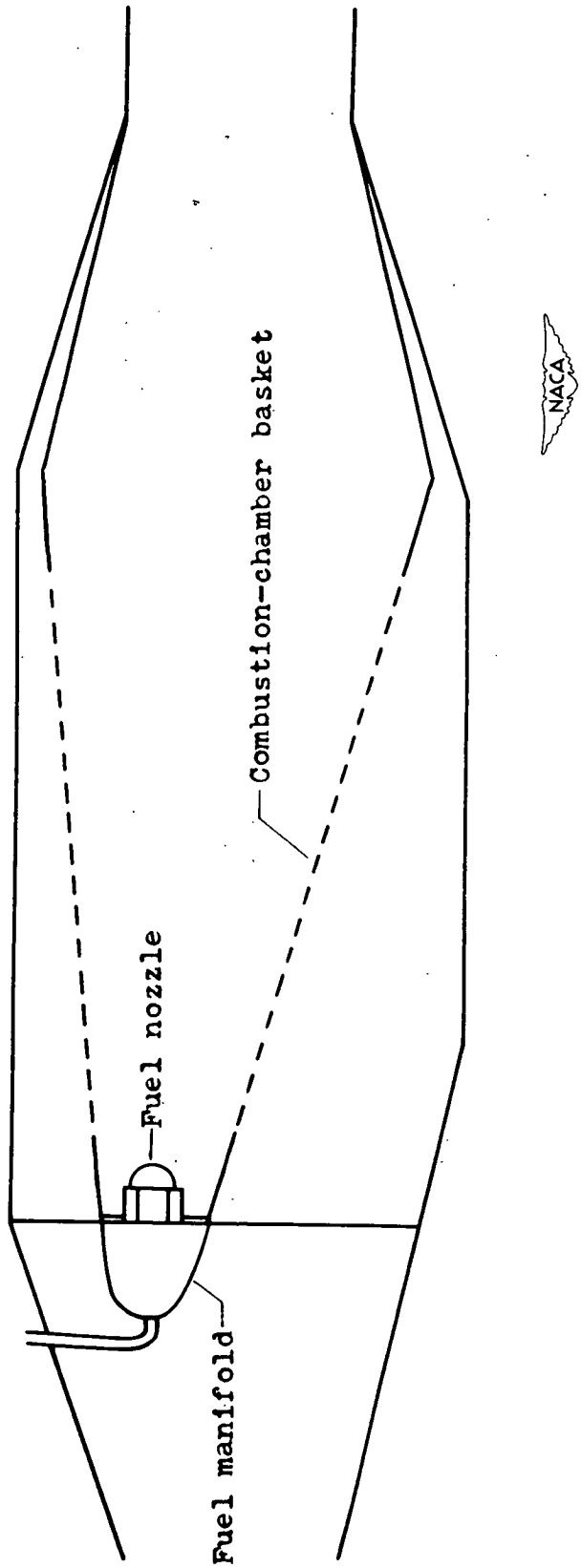

Figure 3. - Schematic view of 198 combustion chamber. Section through one side of annulus.

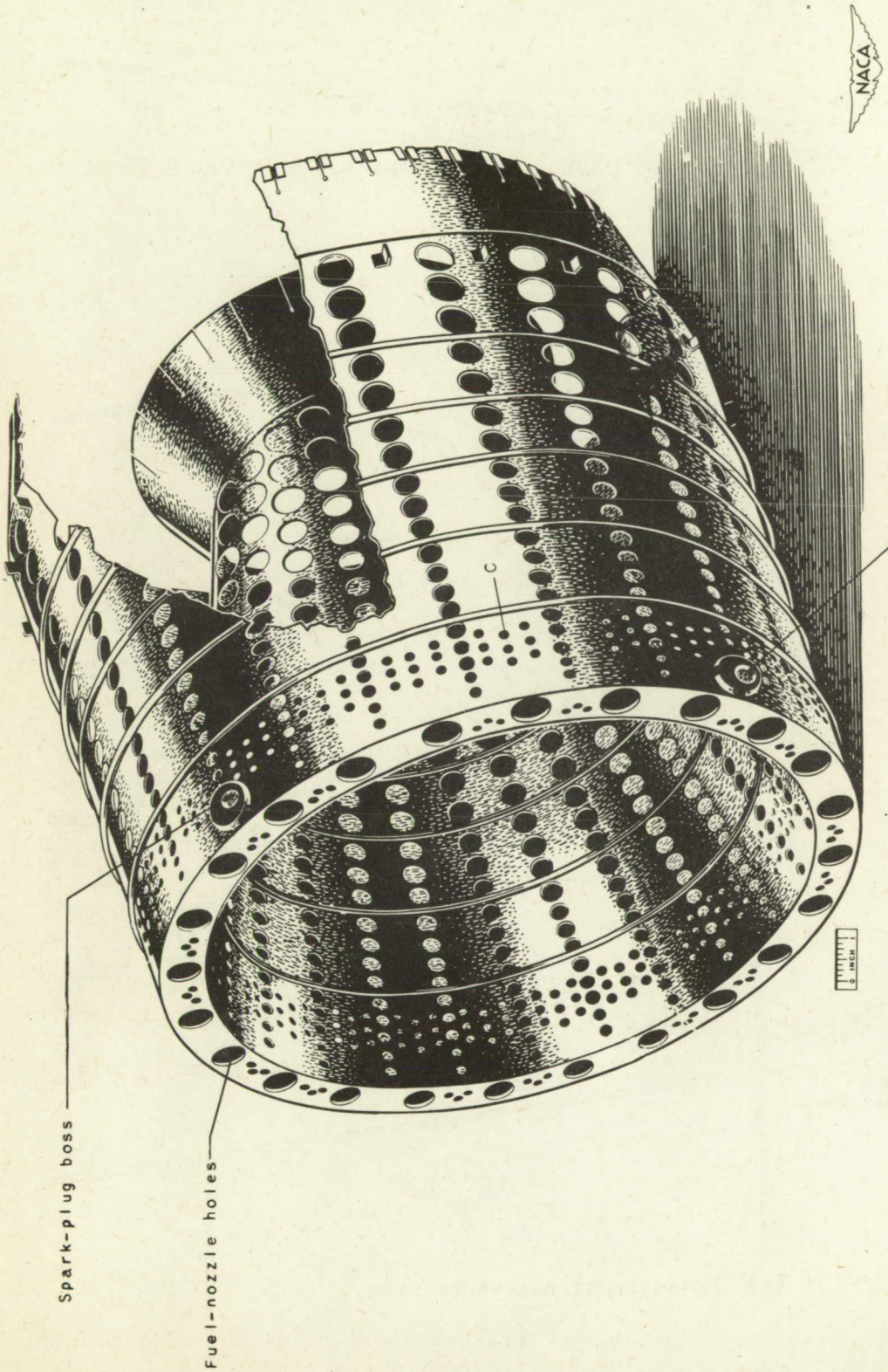

Figure 4. - Combustion-chamber basket of 19B and 19XB-1 jet-propulsion engines.

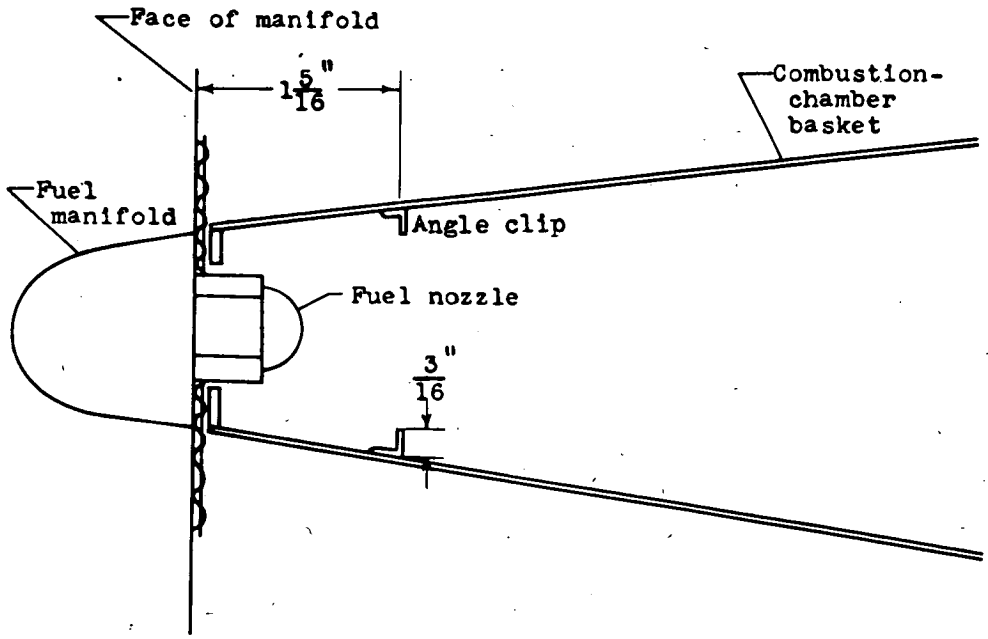

(a) Position of steel angle clips.

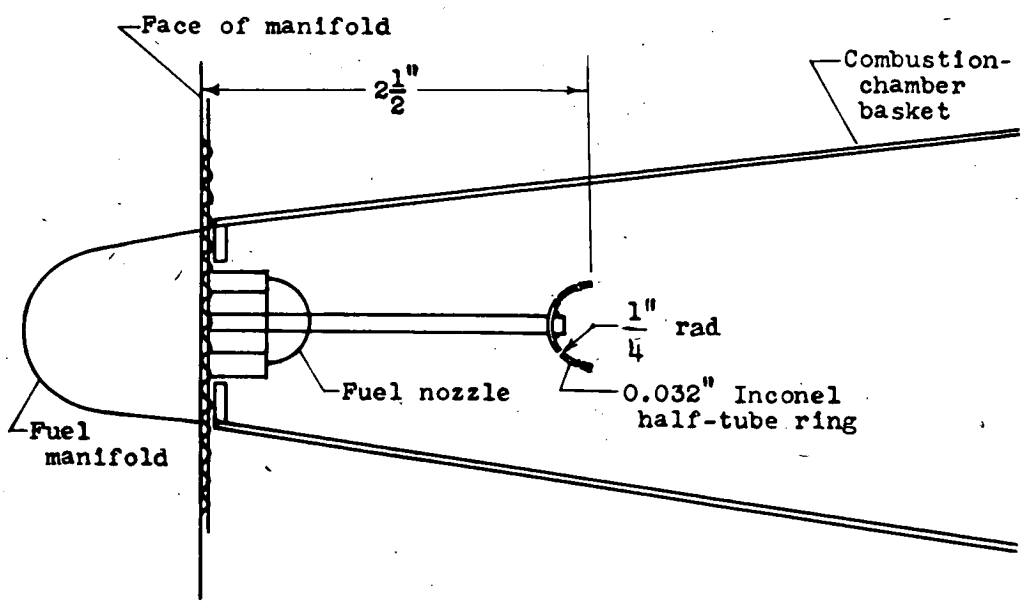

(b) Position of half-tube ring.

Figure 5. - Sketches showing two modifications installed in combustion chamber of 198-2 jet-propulsion engine.

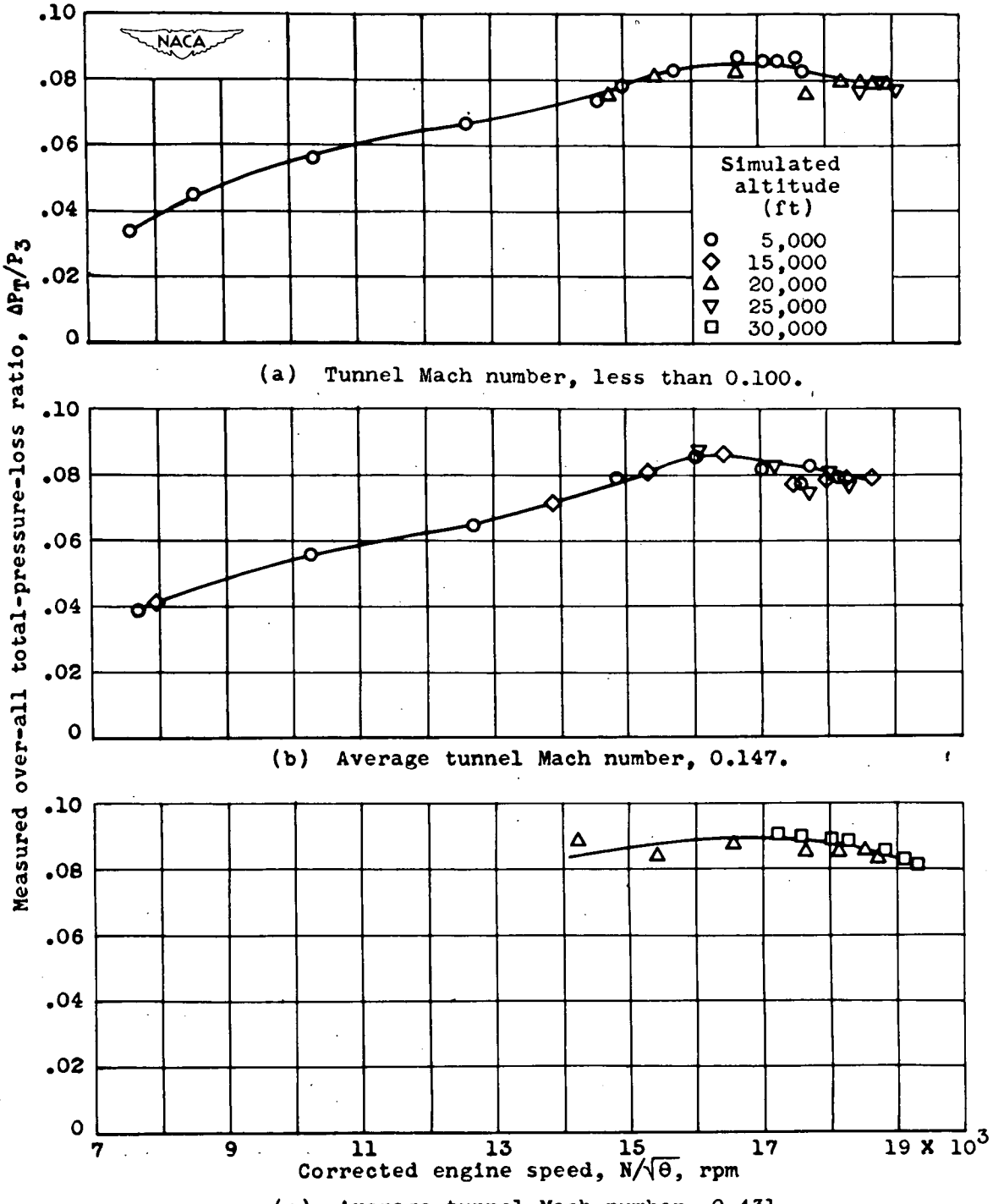

Figure 6. - Relation between measured over-all total-pressure-loss ratio through 198-8 combustion chamber and corrected engine speed for simulated altitudes from 5000 to 30,000 feet. Tail cone in.

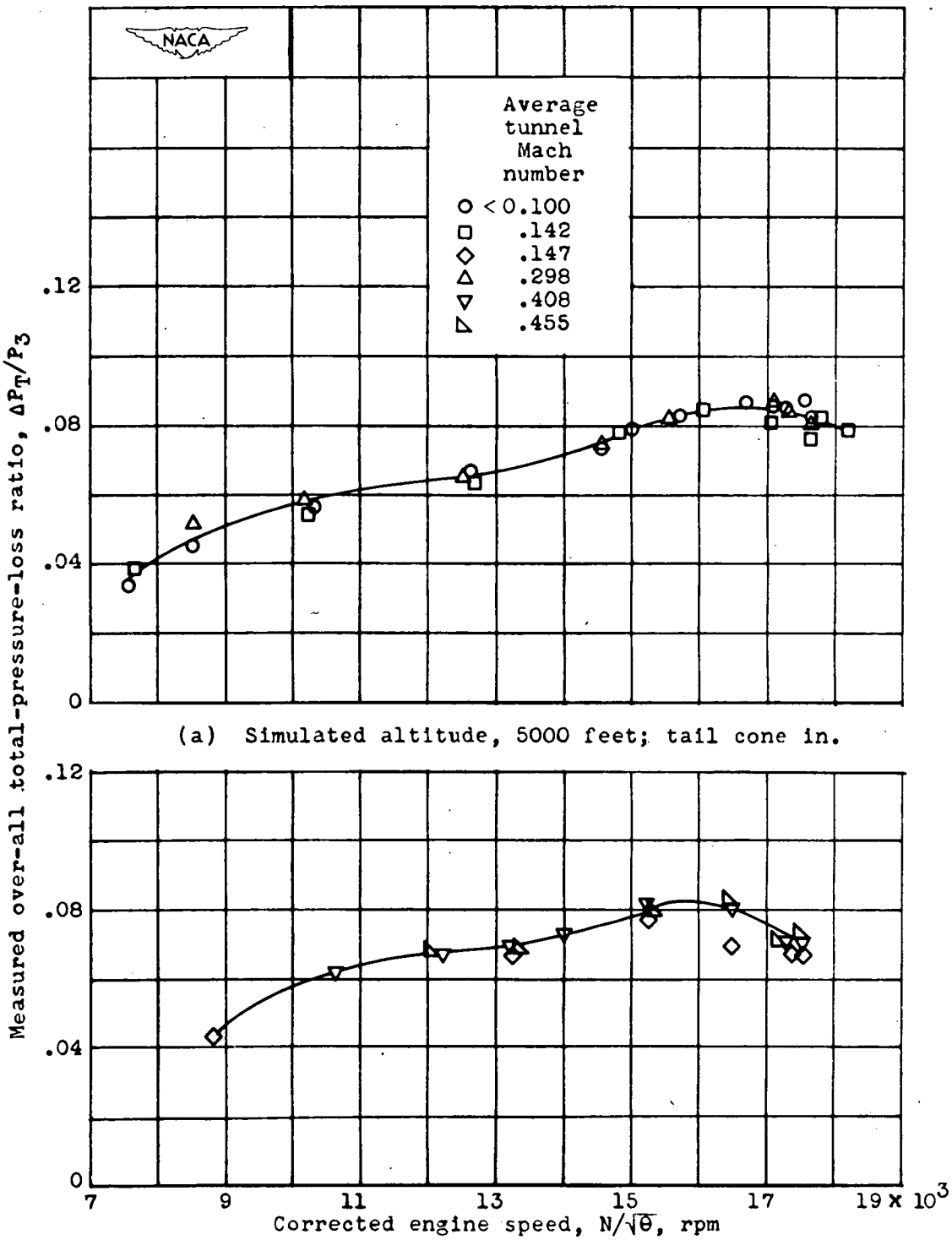

Figure 7. - Relation between measured over-all total-pressure-loss ratio through 19B-8 combustion chamber and corrected engine speed for average tunnel Mach numbers from less than 0.100 to 0.455.

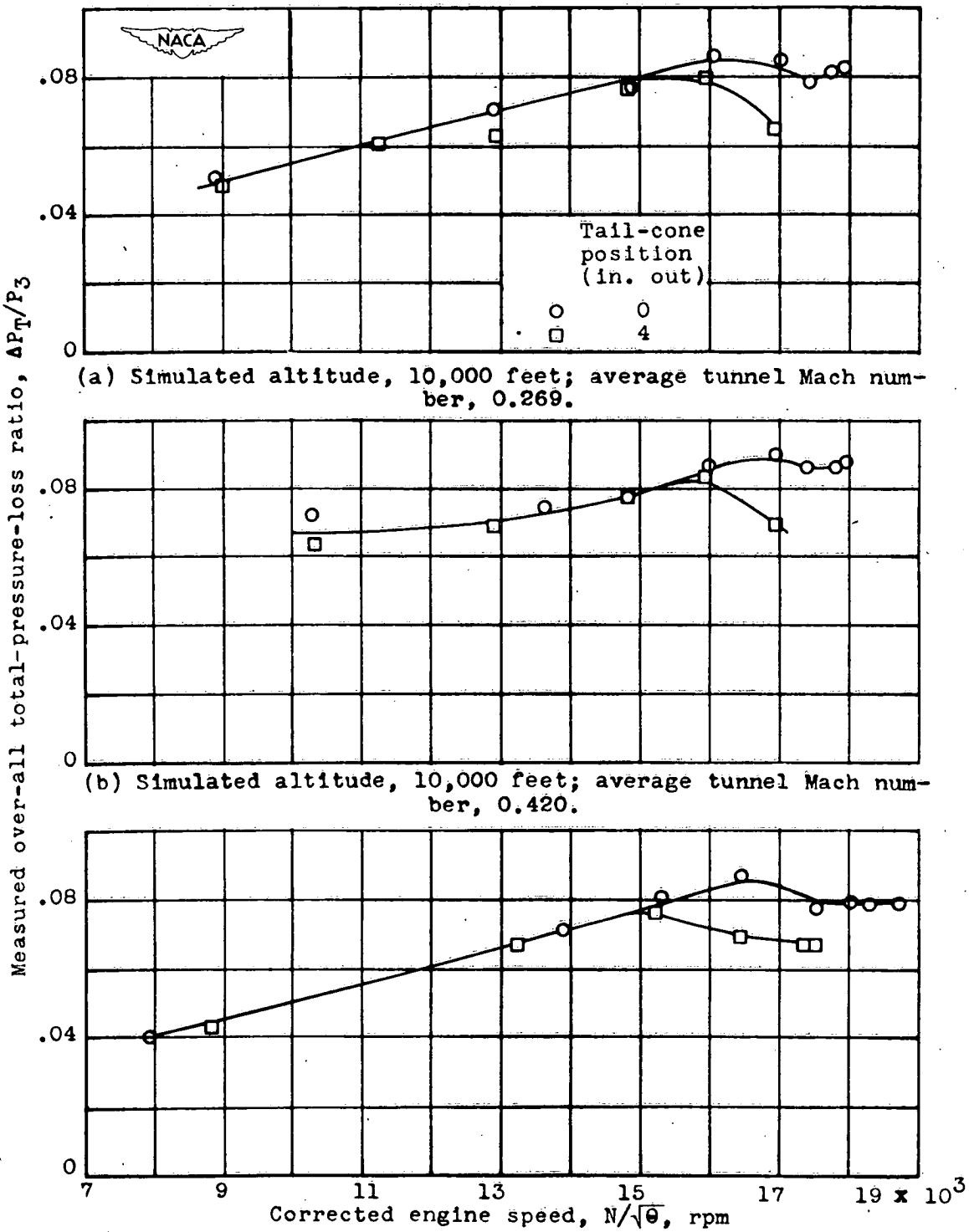

(a) Simulated altitude, 10,000 feet; average tunnel Mach number, 0.269.

(b) Simulated altitude, 10,000 feet; average tunnel Mach number, 0.420.

(c) Simulated altitude, 15,000 feet; average tunnel Mach number, 0.147.

Figure 8. - Relation between measured over-all total-pressure-loss ratio through 198-8 combustion chamber and corrected engine speed with tail cone in and 4 inches out.

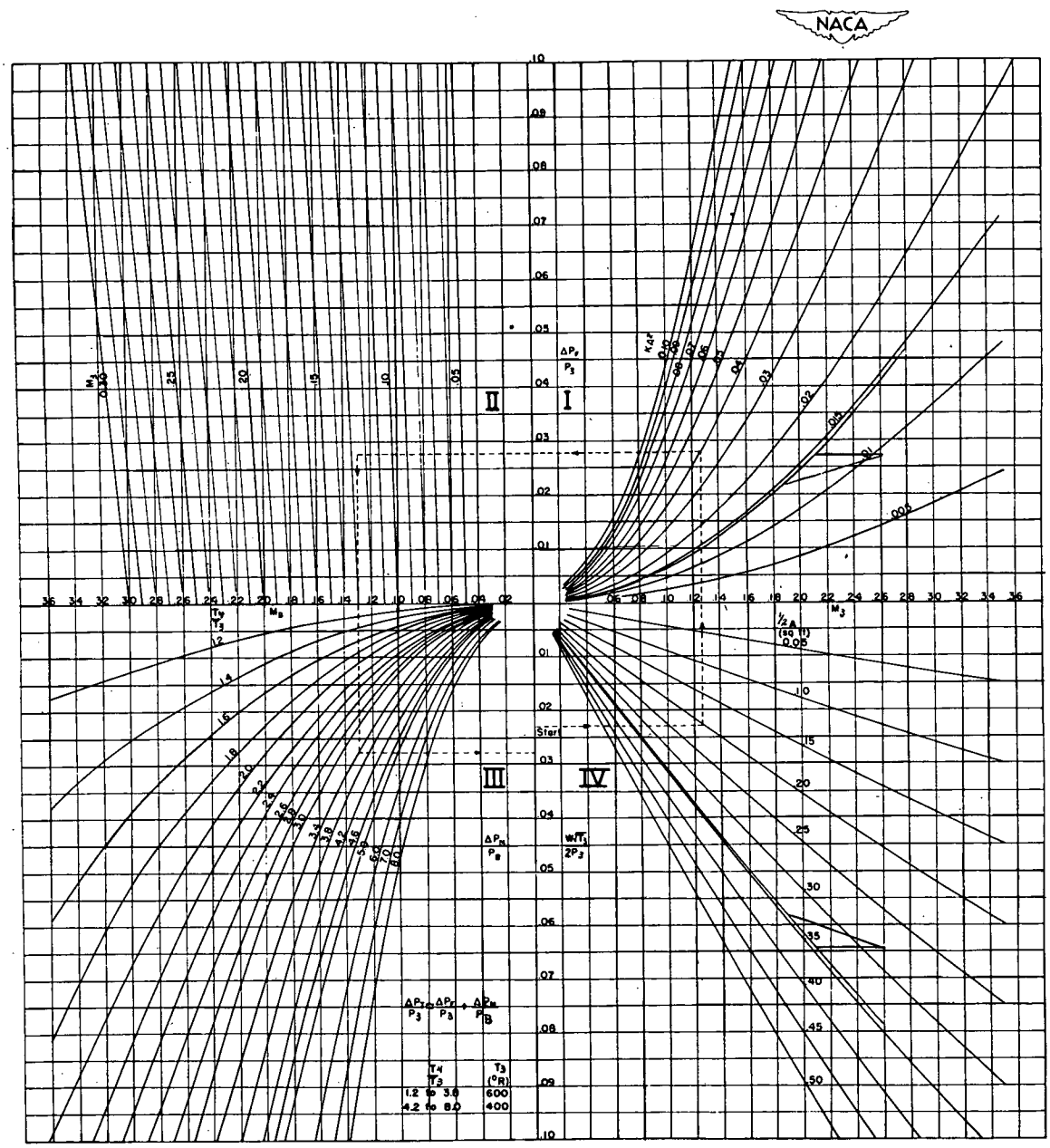

Figure 9. - Combustion-chamber pressure-loss chart. (Based on chart from reference 5.)

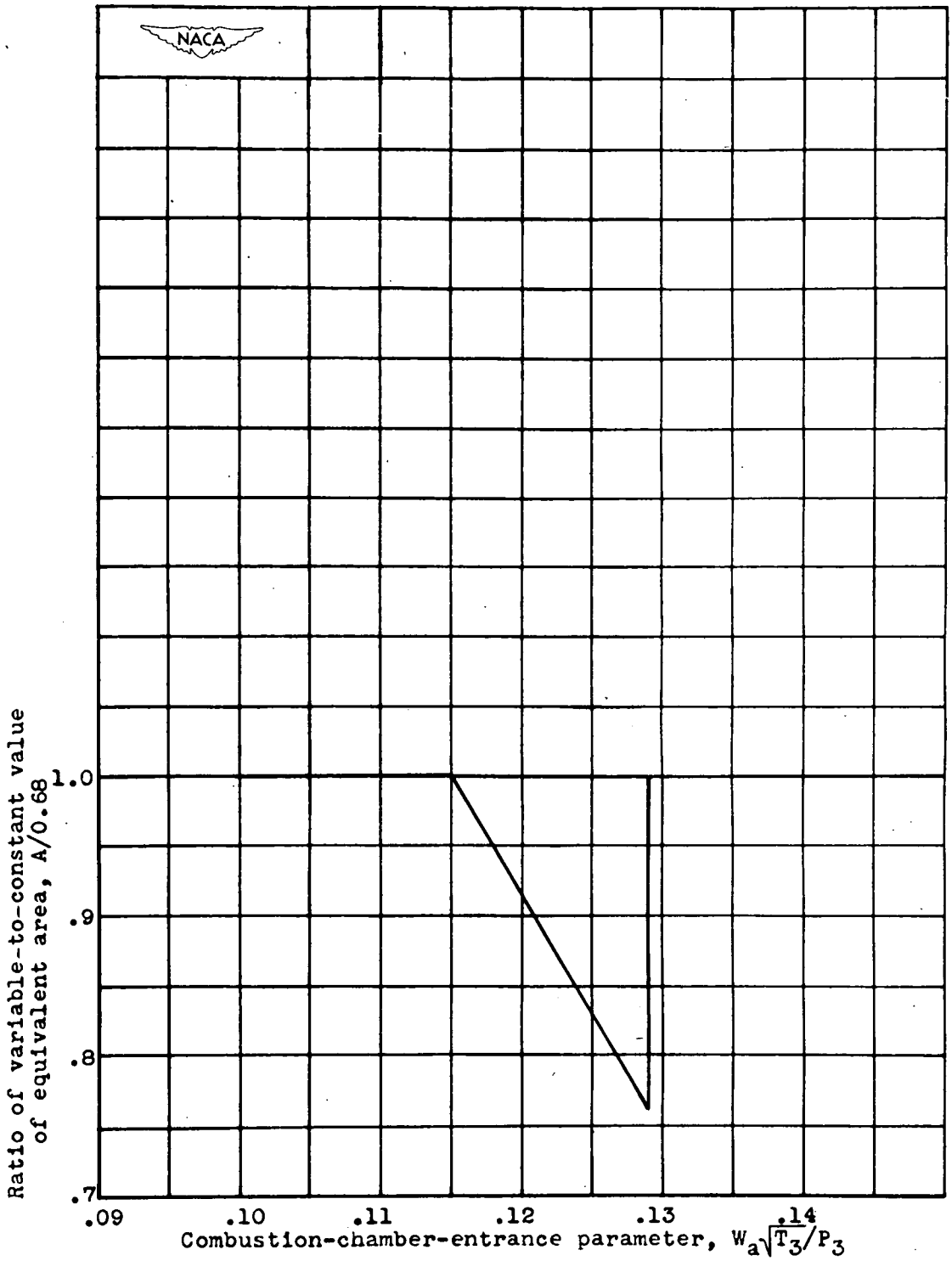

Figure 10. - Variation of equivalent area with combustion-chamber-entrance parameter. 19B-8 turbojet engine.

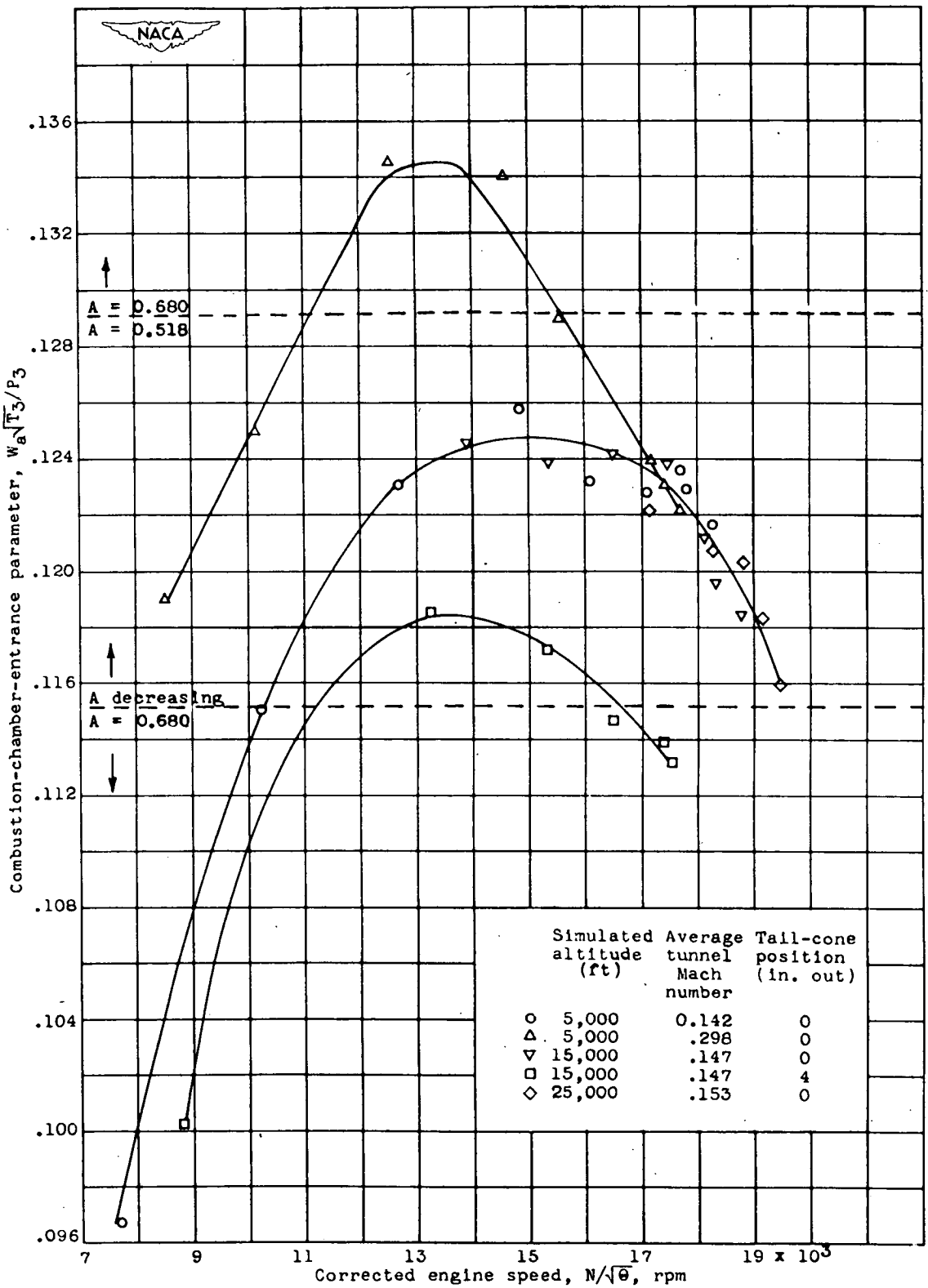

Figure 11. - Relation between combustion-chamber-entrance parameter and corrected engine speed for representative operating conditions. 198-8 turbojet engine.

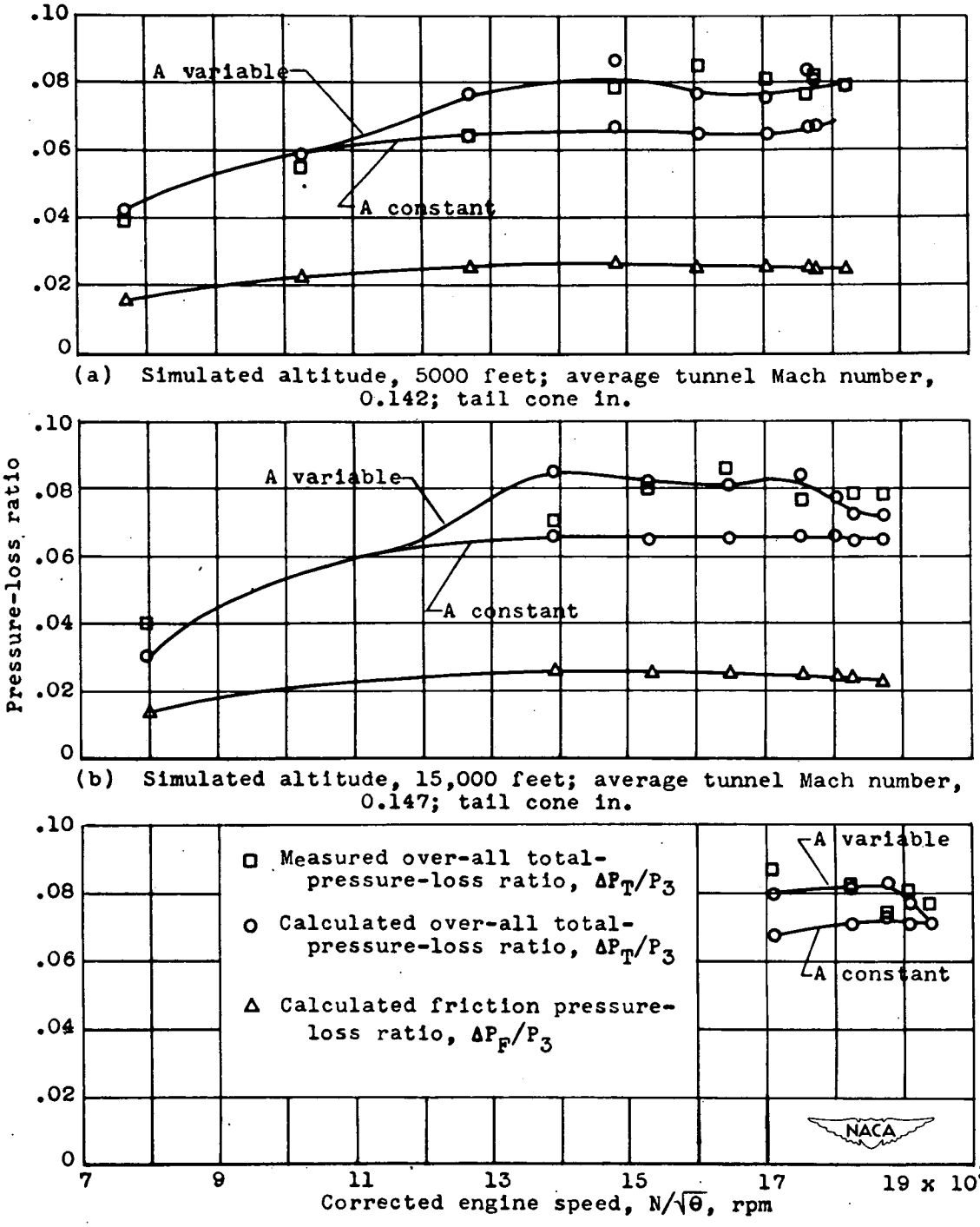

(a) Simulated altitude, 5000 feet; average tunnel Mach number, 0.142; tail cone in.

(b) Simulated altitude, 15,000 feet; average tunnel Mach number, 0.147; tail cone in.

(c) Simulated altitude, 25,000 feet; average tunnel Mach number, 0.153; tail cone in.

Figure 12. - Variation of measured and calculated over-all total-pressure-loss ratios and calculated friction-pressure-loss ratio through 198-8 combustion chamber with corrected engine speed.

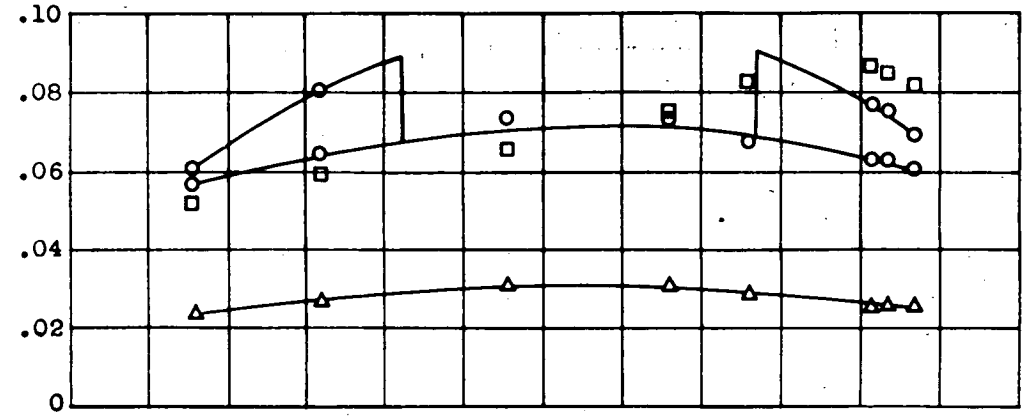

(d) Simulated altitude, 5000 feet; average tunnel Mach number, 0.298; tail cone in.

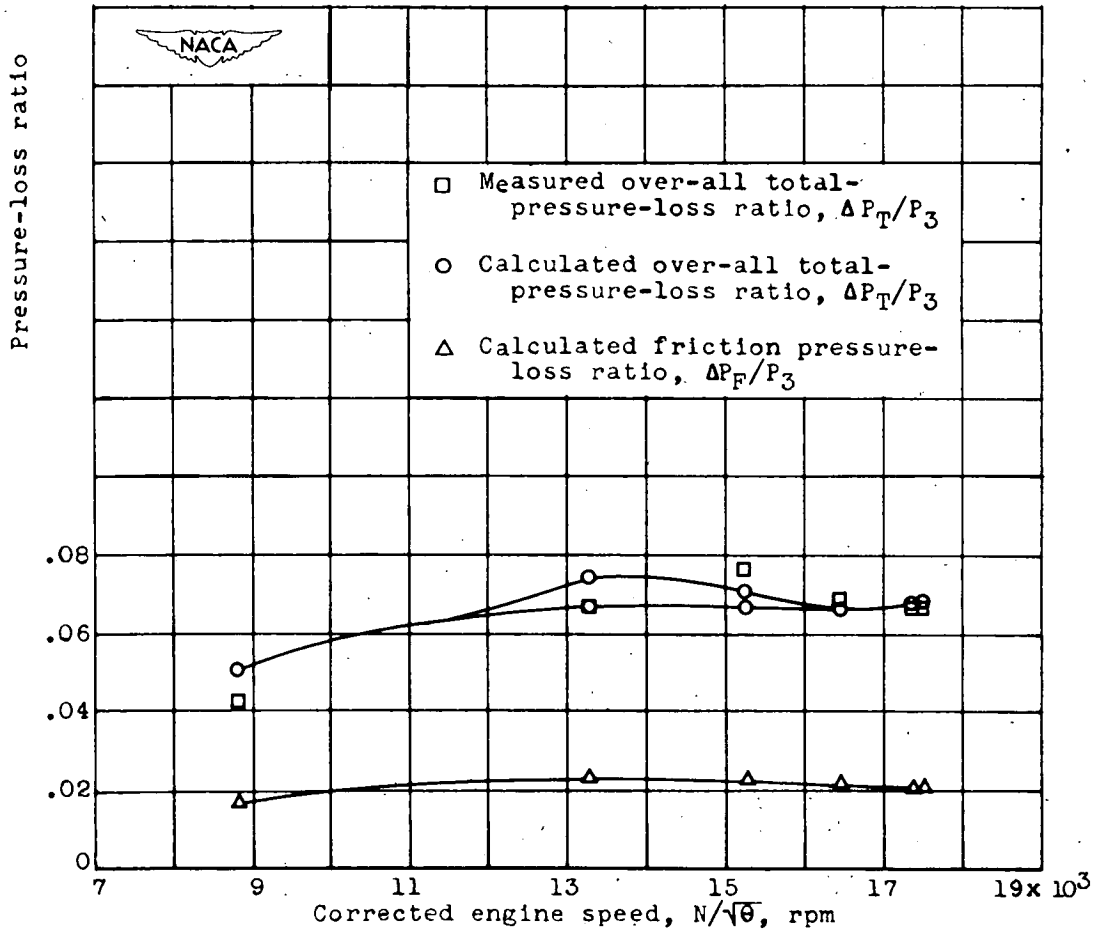

(e) Simulated altitude, 15,000 feet; average tunnel Mach number, 0.147; tail cone 4 inches out.

Figure 12. - Concluded. Variation of measured and calculated over-all total-pressure-loss ratios and calculated friction-pressure-loss ratio through 19B-8 combustion chamber with corrected engine speed.

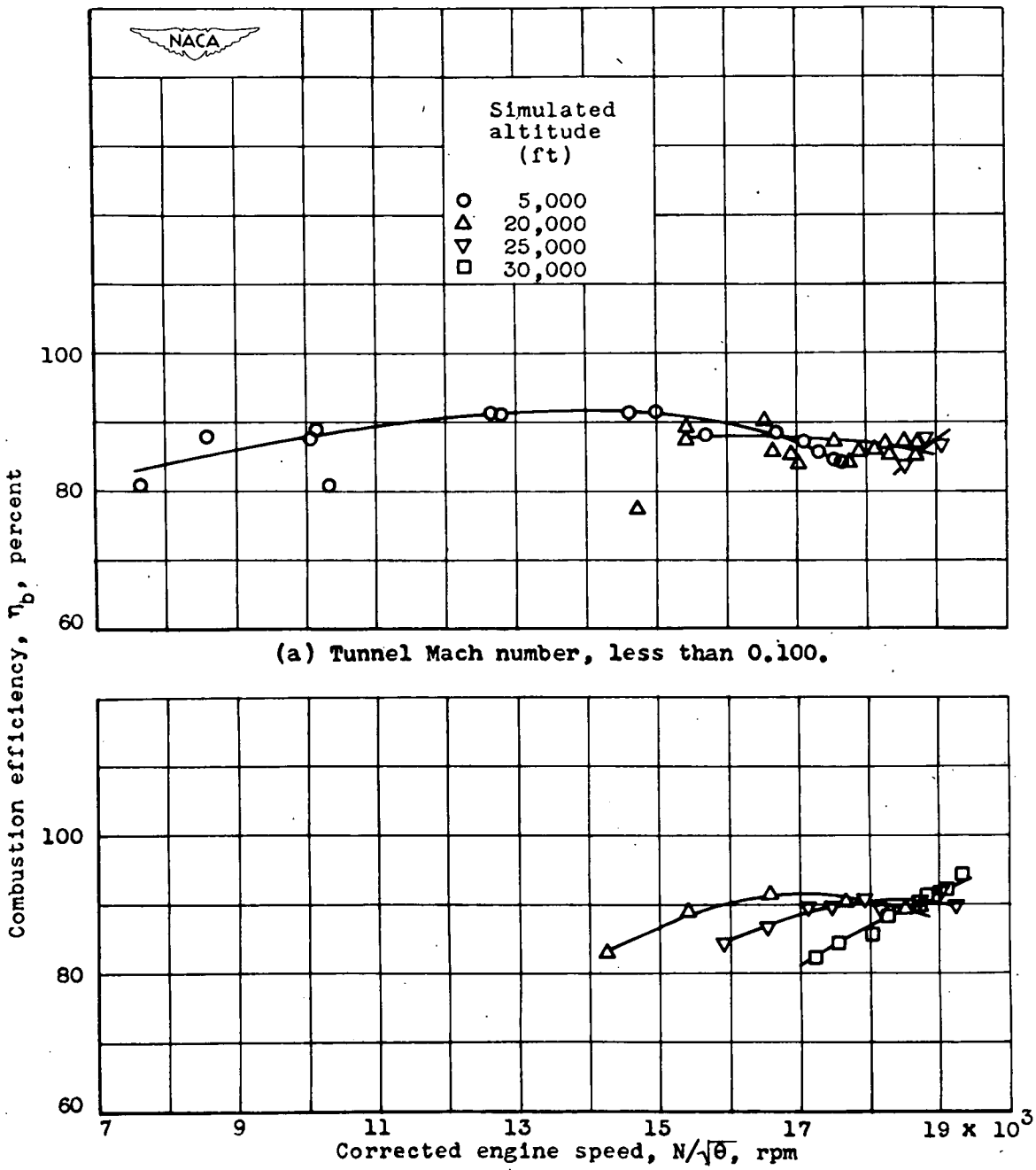

Figure 13. - Relation between combustion efficiency and corrected engine speed for pressure altitudes from 5000 to 30,000 feet. 198-8 turbojet engine; tail cone in.

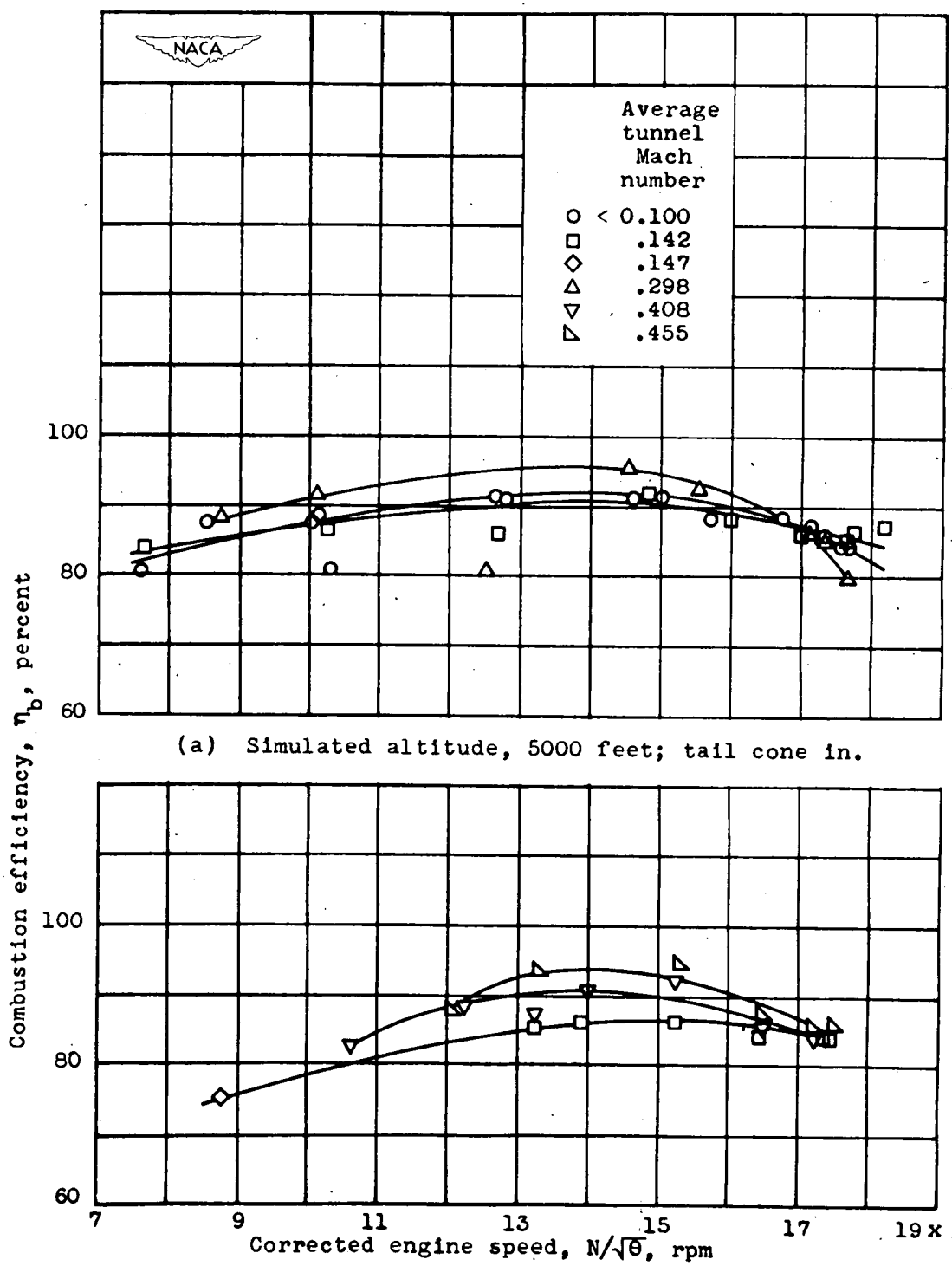

(a) Simulated altitude, 5000 feet; tail cone in.

(b) Simulated altitude, 15,000 feet; tail cone 4 inches out.

Figure 14. - Relation between combustion efficiency and corrected engine speed for average tunnel Mach numbers from less than 0.100 to 0.455. 198-8 turbojet engine.

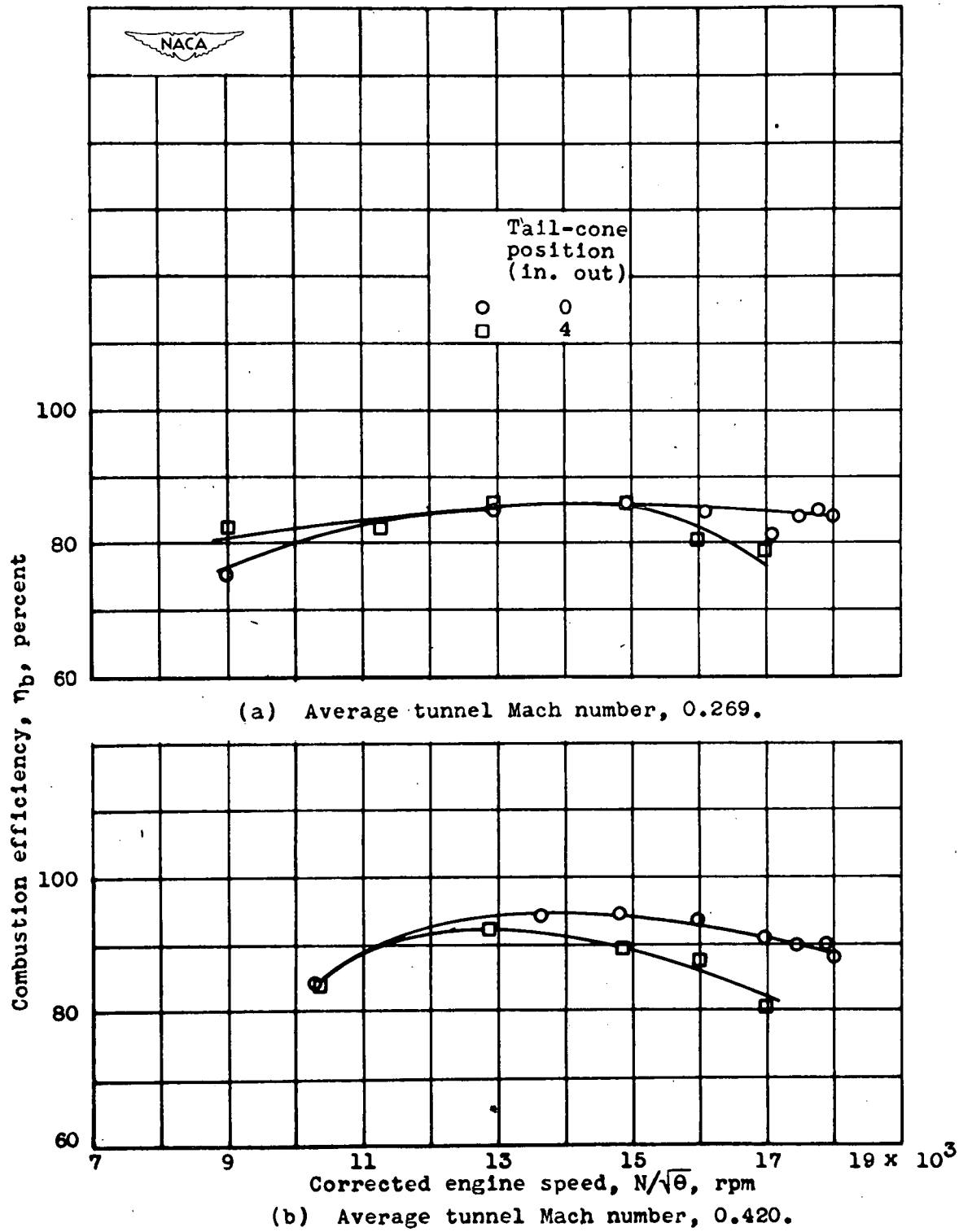

Figure 15. - Relation between combustion efficiency and corrected engine speed with tail cone in and 4 inches out. 19B-8 turbojet engine; simulated altitude, 10,000 feet.

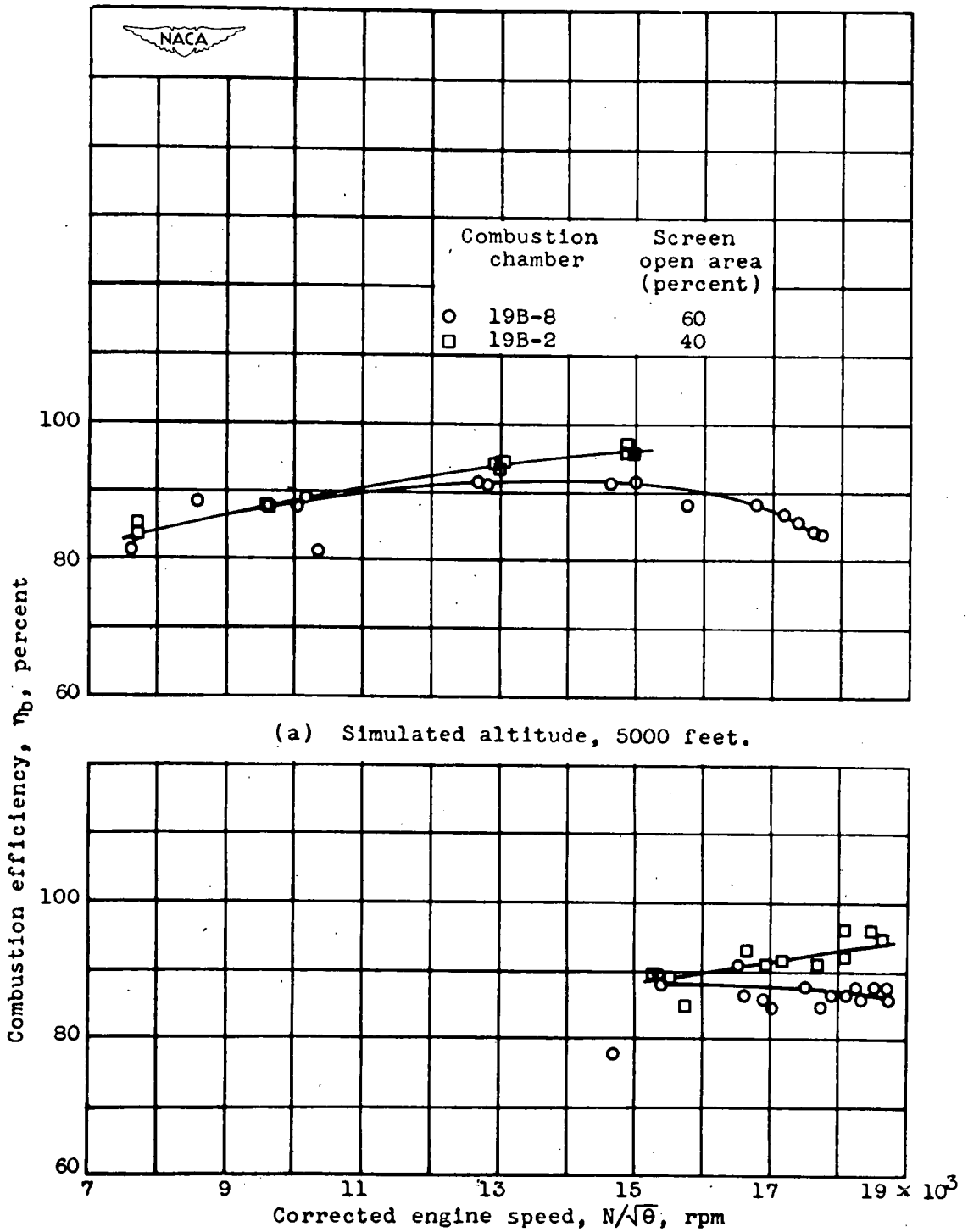

Figure 16. - Comparison of 19B-8 and 19B-2 combustion chambers showing effect of combustion-chamber-inlet screen on combustion efficiency. Tunnel Mach number, less than 0.100; tail cone in.

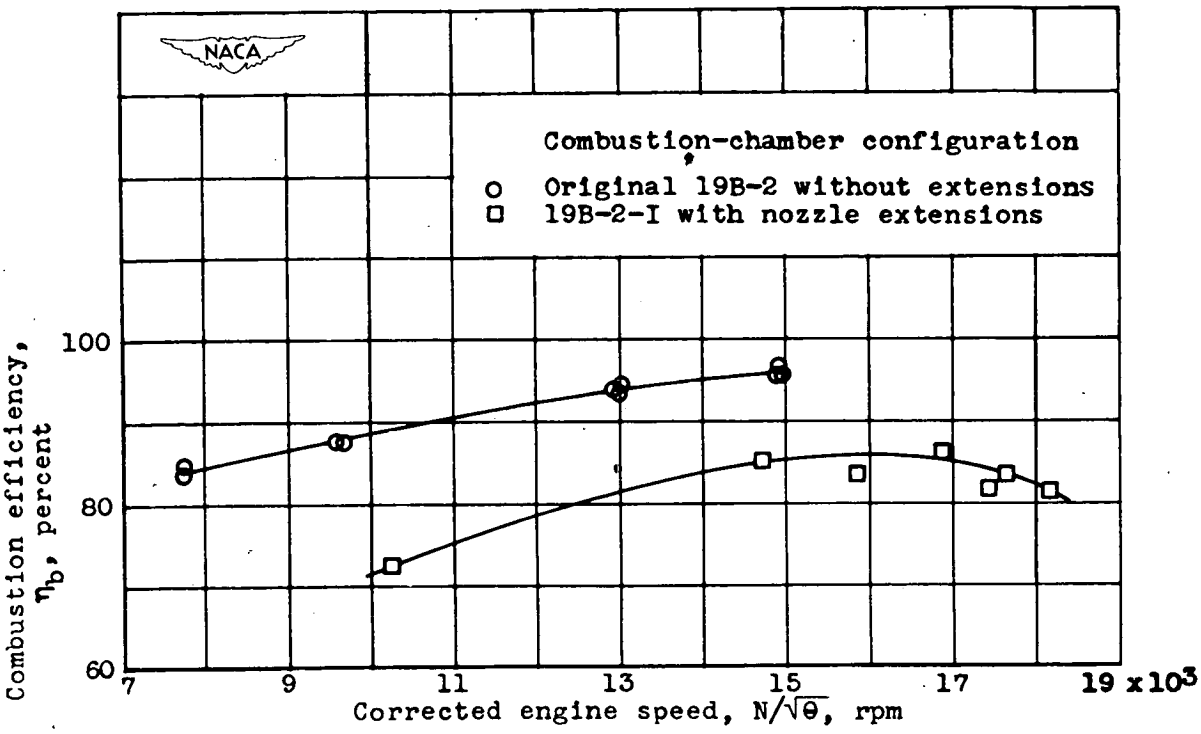

Figure 17. - Comparison of original and modified 19B-2 combustion chambers showing effect of fuel-nozzle extensions on combustion efficiency. Simulated altitude, 5000 feet; tunnel Mach number, less than 0.100; tail cone in.

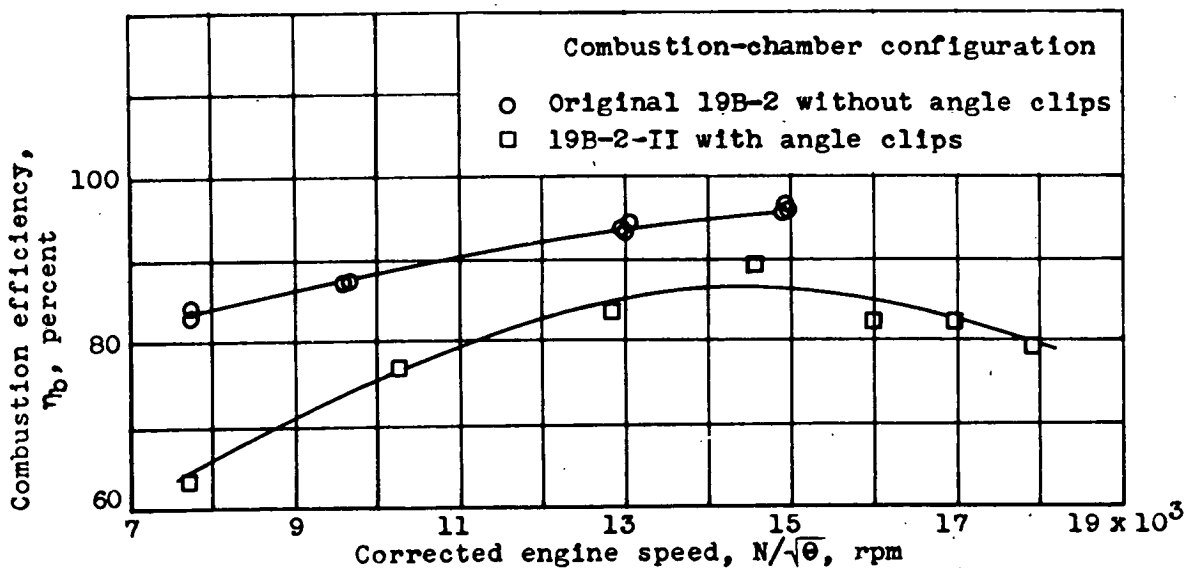

Figure 18. - Comparison of original and modified 19B-2 combustion chambers showing effect of angle clips on combustion efficiency. Simulated altitude, 5000 feet; tunnel Mach number, less than 0.100; tail cone in.

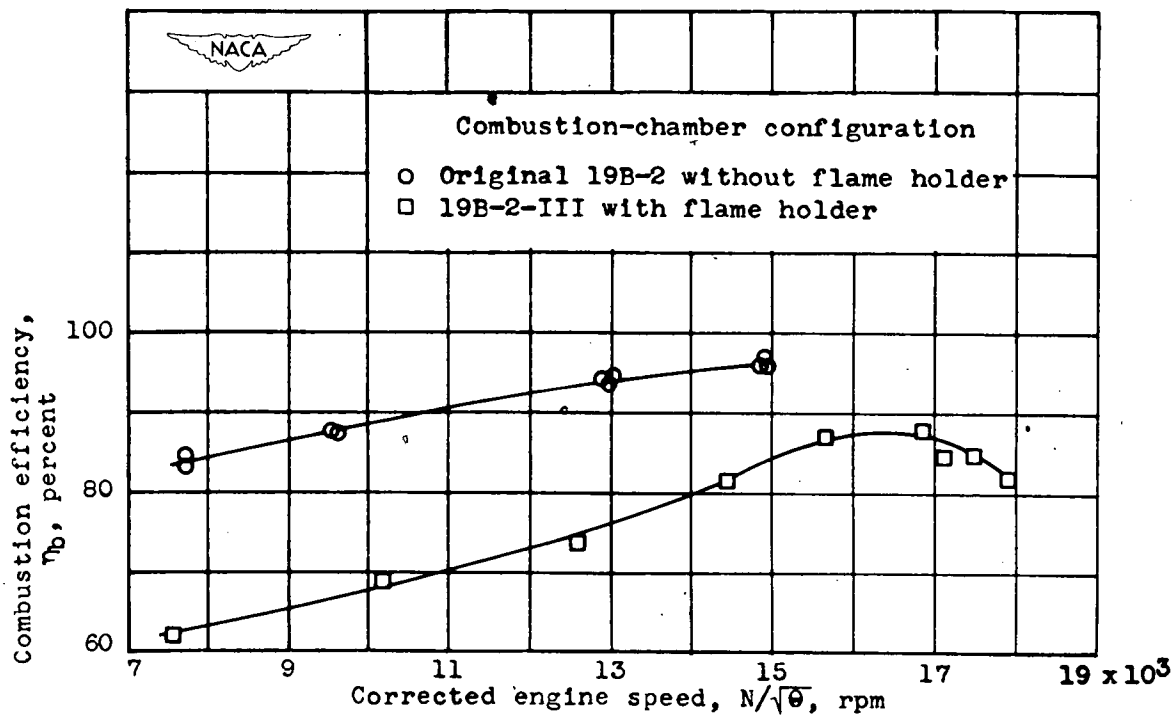

Figure 19. - Comparison of original and modified 19B-2 combustion chambers showing effect of flame holder on combustion efficiency. Simulated altitude, 5000 feet; tunnel Mach number, less than 0.100; tail cone in.

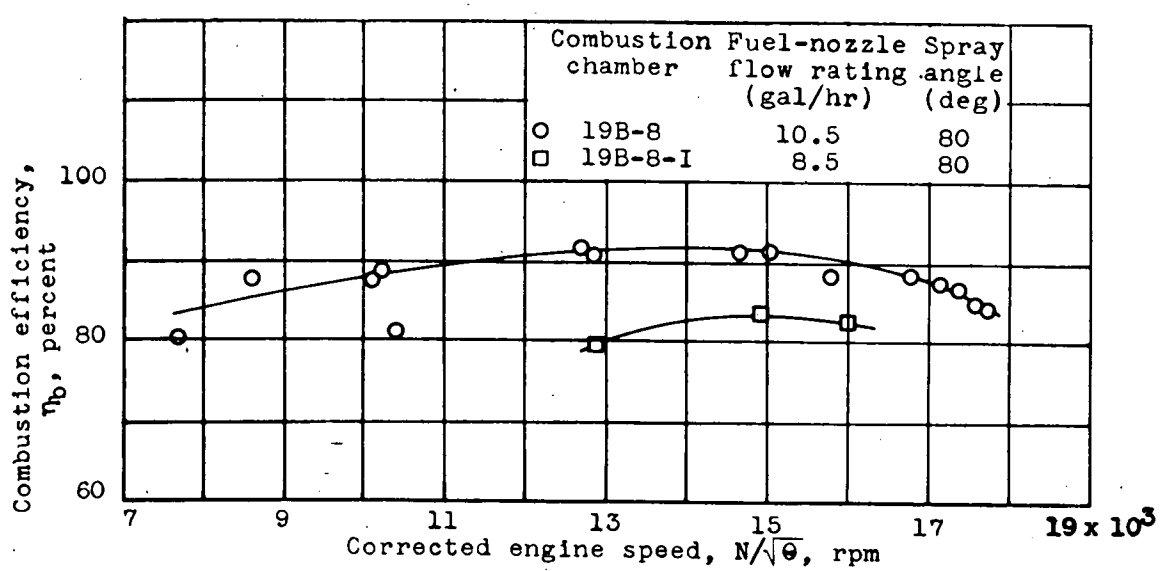

Figure 20. - Comparison of original and modified 19B-8 combustion chambers showing effect of fuel-nozzle flow rating on combustion efficiency. Simulated altitude, 5000 feet; tunnel Mach number, less than 0.100; tail cone in.

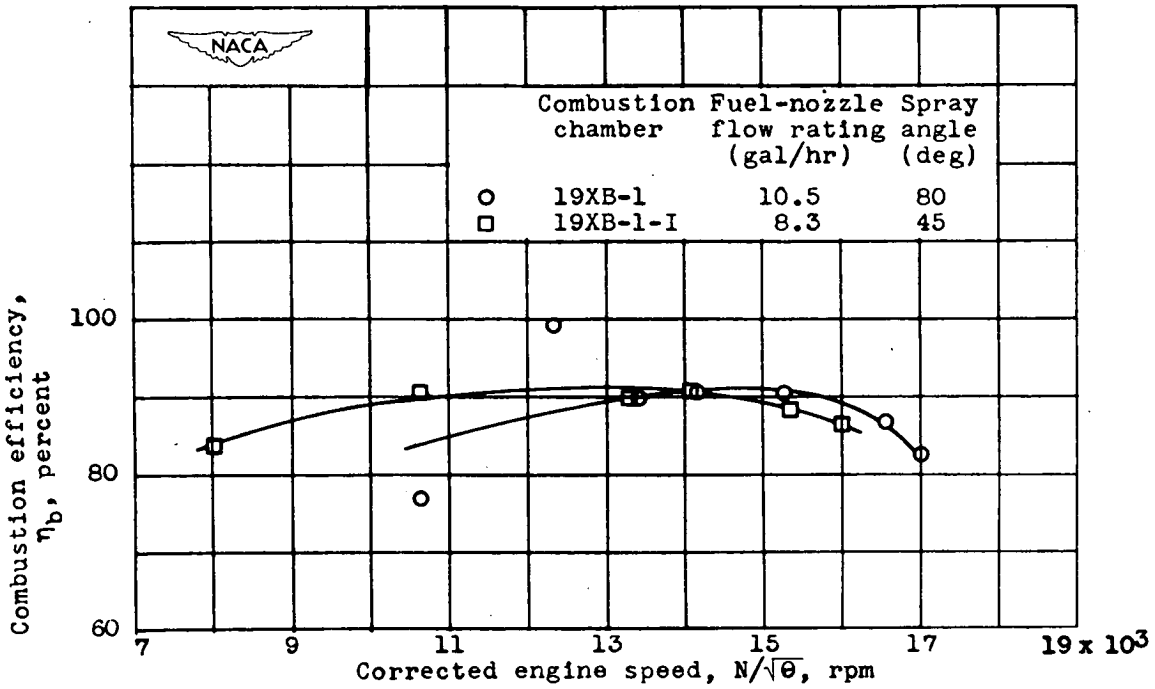

Figure 21. - Comparison of original and modified 19XB-1 combustion chambers showing effect of fuel-nozzle flow rating and spray angle on combustion efficiency. Simulated altitude, 20,000 feet; tunnel Mach number, less than 0.100.

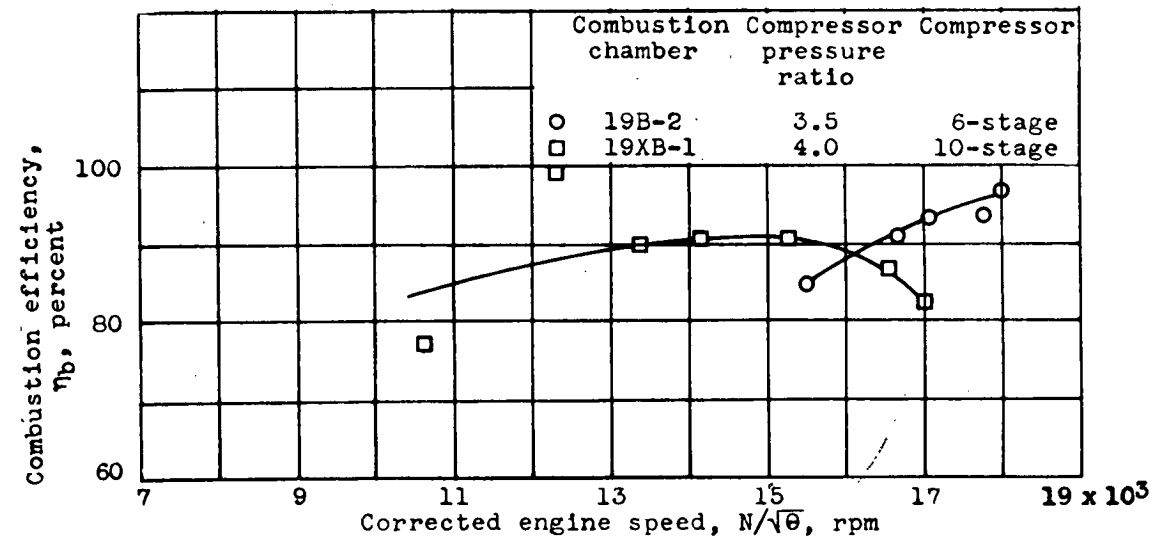

Figure 22. - Comparison of 19B-2 and 19XB-1 combustion chambers showing effect of high-flow compressor on combustion efficiency. Simulated altitude, 20,000 feet; tunnel Mach number, less than 0.100; 19B-2 tail cone 4 inches out.